Intercomparison and validation of the mixed layer depth fields of global ocean syntheses

Article

Accepted Version

Toyoda, T., Fujii, Y., Kuragano, T., Kamachi, M., Ishikawa, Y., Masuda, S., Sato, K., Awaji, T., Hernandez, F., Ferry, N., Guinehut, S., Martin, M. J., Peterson, K. A., Good, S. A., Valdivieso, M., Haines, K., Storto, A., Masina, S., Kohl, A., Zuo, H., Balmaseda, M., Yin, Y., Shi, L., Alves, O., Smith, G., Chang, Y.-S., Vernieres, G., Wang, X., Forget, G., Heimbach, P., Wang, O., Fukumori, I. and Lee, T. (2017) Intercomparison and validation of the mixed layer depth fields of global ocean syntheses. Climate Dynamics, 49 (3). pp. 753-773. ISSN 0930-7575 doi: https://doi.org/10.1007/s00382-015-2637-7 Available at http://centaur.reading.ac.uk/52363/

Title

Intercomparison and validation of the mixed layer depth fields of global ocean syntheses

Authors

Takahiro Toyoda, Yosuke Fujii, Tsurane Kuragano, and Masafumi Kamachi (Meteorological Research Institute, Japan Meteorological Agency (MRI/JMA), Tsukuba, Japan)

Yoichi Ishikawa (Center for Earth Information Science and Technology, Japan Agency for Marine-Earth Science and Technology (CEIST/JAMSTEC), Yokohama, Japan)

Shuhei Masuda, and Kanako Sato (Research and Development Center for Global Change (RCGC), JAMSTEC, Yokosuka, Japan)

Toshiyuki Awaji (CEIST/JAMSTEC, Yokohama, Japan; Kyoto University, Kyoto, Japan)

Fabrice Hernandez (Institut de Recherche pour le Développement (IRD), Toulouse, France; Mercator Océan, Ramonville Sant-Agne, France)

Nicolas Ferry (Mercator Océan, Ramonville Sant-Agne, France)

Stéphanie Guinehut (Collecte Localisation Satellites (CLS), Ramonville Sant-Agne, France)

Matthew Martin, K. Andrew Peterson, and Simon A. Good (Met Office (UKMO), Exeter, UK)

Maria Valdivieso, and Keith Haines (National Centre for Earth Observation (NCEO), Department of Meteorology, University of Reading (U-Reading), Reading, UK)

Andrea Storto (Centro Euro-Mediterraneo sui Cambiamenti Climatici (CMCC), Bologna, Italy)

Simona Masina (CMCC; Istituto Nazionale di Geofisica e Vulcanologia (INGV), Bologna, Italy)

Armin Köhl (Universität Hamburg (U-Hamburg), Hamburg, Germany)

Hao Zuo, and Magdalena Balmaseda (European Centre for Medium-Range Weather Forecasts

(ECMWF), Reading, UK)

Yonghong Yin, Li Shi, and Oscar Alves (Centre for Australian Weather and Climate Research, Bureau of Meteorology (BOM), Melbourne, Australia)

Gregory Smith (Environment Canada, Québec, Canada)

You-Soon Chang (Geophysical Fluid Dynamics Laboratory, National Oceanic and Atmospheric Administration (GFDL/NOAA), Princeton, New Jersey, USA; Kongju National University, Kongju, South Korea)

Guillaume Vernieres (Science System and Applications, Inc., Lanham, Maryland, USA; Global Modeling and Assimilation Office, National Aeronautics and Space Administration Goddard Space Flight Center (GSFC/NASA/GMAO), Greenbelt, Maryland, USA)

Xiaochun Wang (Joint Institute for Regional Earth System Science and Engineering, University of California, Los Angeles, California, USA)

Gael Forget, and Patrick Heimbach (Department of Earth, Atmospheric and Planetary Sciences, Massachusetts Institute of Technology (MIT), Cambridge, Massachusetts, USA)

Ou Wang, Ichiro Fukumori, and Tong Lee (Jet Propulsion Laboratory (JPL), California Institute of Technology, Pasadena, California, USA)

Corresponding author

Takahiro Toyoda, Oceanography and Geochemistry Research Department, Meteorological Research Institute, Japan Meteorological Agency, 1-1 Nagamine, Tsukuba, 305-0052, Japan

E-mail: ttoyoda@mri-jma.go.jp

Abstract

Intercomparison and evaluation of the global ocean surface mixed layer depth (MLD) fields estimated from a suite of major ocean syntheses are conducted. Compared with the reference MLDs calculated from individual profiles, MLDs calculated from monthly mean and gridded profiles show negative biases of 10-20 m in early spring related to the re-stratification process of relatively deep mixed layers. Vertical resolution of profiles also influences the MLD estimation. MLDs are underestimated by approximately 5-7 (14-16) m with the vertical resolution of 25 (50) m when the criterion of potential density exceeding the 10-m value by 0.03 kg m^{-3} is used for the MLD estimation. Using the larger criterion (0.125 kg m^{-3}) generally reduces the underestimations. In addition, positive biases greater than 100 m are found in wintertime subpolar regions when MLD criteria based on temperature are used. Biases of the reanalyses are due to both model errors and errors related to differences between the assimilation methods. The result shows that these errors are partially cancelled out through the ensemble averaging. Moreover, the bias in the ensemble mean field of the reanalyses is smaller than in the observation-only analyses. This is largely attributed to comparably higher resolutions of the reanalyses. The robust reproduction of both the seasonal cycle and interannual variability by the ensemble mean of the reanalyses indicates a great potential of the ensemble mean MLD field for investigating and monitoring upper ocean processes.

Keywords

ocean reanalysis, mixed layer depth, Ocean Reanalyses Intercomparison Project (ORA-IP), data assimilation, ocean general circulation model, isothermal layer depth

1 Introduction

The ocean surface mixed layer (ML), directly communicating with the atmosphere, transmits surface heat, freshwater and momentum fluxes to the interior ocean, which forces the ocean circulation (e.g., Pedlosky 1996). On the other hand, sea surface temperature (SST), which provides the boundary condition for the atmosphere, is determined through the ML processes. Also, heat content in the ML is one of the primary forcing factors of the atmospheric circulation in some cases (e.g., Shey et al. 2000). Since the ML depth (MLD) is a relevant physical parameter for describing the dynamic nature of the ML, it is of great value to quantitatively determine the spatio-temporal variation of the MLD in the global ocean for better understanding the ocean circulation and air-sea interaction.

The Ocean Reanalyses Intercomparison Project (ORA-IP) was initiated to evaluate global ocean syntheses produced in several research and operational centers (Balmaseda et al. 2015). These syntheses include both analyses that use observations only and analyses that combine ocean models and observations through data assimilation methods (referred to as "reanalyses" in this study). It is important to evaluate their strength and weakness in various aspects in order to understand the extent to which these products can be used to monitor the state of the ocean, initialize climate prediction and understand oceanic physical processes and in order also to identify priorities for new developments (e.g., Lahoz and Errera 2010). Furthermore, the signal-to-noise ratio inferred from an ensemble of these products can improve the understanding of the robustness of oceanic physical processes represented by these reanalyses (e.g., Lee et al. 2009).

MLD is selected as one of the important indices for the ORA-IP (Toyoda et al. 2014) in addition

to heat and salt content, steric height, sea level, surface heat fluxes, depth of the 20 degree isotherm and sea ice. In the present study, monthly mean global MLD time series are estimated and intercompared from 19 syntheses (2 observation-only analyses and 17 reanalyses). Following a brief description of MLDs in Sect. 2, we first investigate the observation-only analyses focusing on errors in estimating MLDs in Sect. 3. The ensemble mean of the reanalyses is also examined since it can have a better fidelity in some regions if model errors in the individual reanalyses cancel out through the ensemble averaging approach. Intercomparisons of all the syntheses/reanalyses are provided in Sect. 4. The findings are summarized in Sect. 5.

2 Data

2.1 Definition of MLD

For the MLD definition, density criteria (e.g., Levitus 1982) are used in this study, i.e., MLD is defined as the depth where potential density exceeds the 10-m depth value by $\Delta\rho = 0.03$ or 0.125 kg m^{-3} ("MLDr003"/"MLDr0125"), since these 2 criteria are often used (e.g., Hosoda et al. 2010) and our interest is in sensitivity of the MLD estimation to the criterion value. Similarly, isothermal layer depth (ILD) is defined as the depth where potential temperature differs from the 10-m depth value by $\Delta T = 0.2$ºC or 0.5ºC ("ILDt02"/"ILDt05"). These ILDs were sometimes used as substitutes for MLDs in previous studies since salinity profiles are less numerous than temperature profiles. Hence, for the present intercomparison, both MLDs and ILDs are used as indices for vertical mixing intensity in the upper ocean. Note that the above

121 temperature criterion ($\Delta T = 0.5$ºC), multiplied by the characteristic thermal expansion rate (e.g.,
122 0.24 kg m^{-3} ºC^{-1} at 18ºC and 35 psu), generally correspond to the density criterion ($\Delta\rho = 0.125$
123 kg m^{-3}).
124
125 **2.2 Observation-only analyses**
126
127 Two observation-only analyses archived in the ORA-IP are used in this study, EN3v2a and
128 ARMOR3D (Table 1). EN3v2a analyzed in-situ temperature and salinity (TS) observations;
129 ARMOR3D synthesized satellite-derived sea level anomalies (SLAs) and SSTs in addition to in-
130 situ TS observations. Monthly MLD and ILD time series are calculated from the monthly mean
131 TS fields on the native grids of the individual datasets. Interpolated values on global longitude-
132 latitude grids with one-degree resolution are used for the intercomparison.
133
134 In order to evaluate the MLDs/ILDs in the ORA-IP, we use the freely available MLD/ILD
135 datasets of MILA-GPV (Hosoda et al. 2010) and de Boyer Montégut et al. (2004; "deBoyer"
136 hereafter). These data are estimated as the average of MLDs/ILDs deduced from individual TS
137 profiles. In particular, MILA-GPV uses only the Argo profiles without interpolation between
138 grid points, although the spatio-temporal coverage of the dataset is limited. Hence, we use
139 MILA-GPV as a reference for the intercomparison mainly (e.g., Fig. 1). Note that deBoyer
140 provides only the monthly climatological fields for MLDr003 and ILDt02.
141
142 Additionally, we use MLDs/ILDs calculated from the monthly TS climatologies of the World
143 Ocean Atlas (WOA) 2009 (e.g., Locarnini et al. 2010). Note that this dataset (derived from TS
144 climatologies) is somewhat similar to EN3v2a and ARMOR3D (derived from monthly TS

145 analyses) but different from MILA-GPV and deBoyer (derived from individual TS profiles).

146

147 **2.3 Reanalyses**

148

149 Each of the reanalyses used in this study may have their own systematic error, attributed to
150 ocean general circulation model (OGCM), spatial resolution, surface forcing, ML
151 parameterization, assimilated data and assimilation method adopted in each analysis (Table 2).
152 The ensemble averaging will partially result in compensation of errors, thus decreasing the error
153 of the MLD estimate, but still errors will remain. In addition, the reanalyses can be clustered in
154 several groups: For example, versions of NEMO are used in G2V3, C-GLORS, UR025.4,
155 GloSea5, ORAS4 and ORAP5, while versions of MOM are used in MERRA, ECDA, PEODAS,
156 K7-ODA and K7-CDA; Smoother approaches are adopted in GECCO2, ECCO-NRT, ECCO-v4,
157 K7-ODA and K7-CDA; Coupled models are used in ECDA, K7-CDA and MOVE-C; Relatively
158 high horizontal resolutions are adopted in G2V3, C-GLORS, UR025.4, GloSea5, ORAP5 and
159 ECCO-v4. If similar MLD features are exhibited within the groups, important information for
160 improving the systems can be provided.
161 As for the observation-only analyses, monthly MLD and ILD time series are calculated from the
162 monthly mean TS fields on the native grids and interpolated onto the common longitude-latitude
163 grids with one-degree resolution.

164

165 In addition, the ensemble mean of the 17 model based reanalysis MLDs/ILDs are calculated
166 ("ENSMEAN"; not including EN3v2a and ARMOR3D). Note that these MLDs/ILDs differ
167 from MLDs/ILDs calculated from the ensemble mean TS fields. In order to reduce the influence
168 of the difference in period among the reanalyses (Table 3), the MLD/ILD time series for

ENSMEAN are calculated as follows: Monthly climatologies averaged over the period of 2001-2011 (or longest available during this period hereafter) and monthly interannual anomalies from these climatologies are first computed for the individual ensemble members. Using these climatologies and interannual anomalies, the monthly climatologies and interannual anomalies (for 1948-2012) of ENSMEAN are calculated respectively. The absolute MLD/ILD time series for ENSMEAN are produced as the sum of these monthly climatologies and interannual anomalies.

3 Uncertainties in observation-only analyses

Figure 1 exhibits the zonal-mean monthly MLD/ILD normalized differences of EN3v2a, ARMOR3D, deBoyer, WOA and ENSMEAN from MILA-GPV. (Note that this does not mean that MILA-GPV is true.) The differences between deBoyer and MILA-GPV (MLDr003 and ILDt02) are generally small, since these are comparable datasets that use individual TS profiles. Relatively large differences at high latitudes may possibly result from spatio-temporally limited observations there, especially from the Argo floats. MLDs/ILDs for WOA, EN3v2a and ARMOR3D exhibit biases toward shallower depths. ILDt02s in WOA are 20 to 40% shallower than those in MILA-GPV globally, which is consistent with the result of de Boyer Montégut et al. (2004). They indicated that the global shallow biases are attributed to the fact that MLD/ILD calculated from averaged TS profiles is more strongly affected by profiles from which shallower MLD/ILD are estimated. Therefore, it can be considered that the smaller discrepancies from MILA-GPV for EN3v2a and ARMOR3D than those for WOA, as shown in Fig. 1, are due to their use of the monthly mean TS profiles as opposed to the climatologically averaged TS

profiles as in WOA.

As described above, the temperature criterion ($\Delta T = 0.5^{o}C$) generally correspond to the density criterion ($\Delta\rho = 0.125$ kg m^{-3}). These criteria give similar patterns for each of the observation-only analyses except that large positive biases are seen at about 60ºS-40ºS and 40ºN-60ºN in winter-early spring for the temperature criterion cases. We will discuss these biases later (subsection 3.3).

By using larger values for the criterion ($\Delta\rho = 0.125$ kg m^{-3} and $\Delta T = 0.5^{o}C$), generally similar patterns to those with smaller values ($\Delta\rho = 0.03$ kg m^{-3} and $\Delta T = 0.2^{o}C$) are obtained for WOA, EN3v2a and ARMOR3D, respectively, but the amplitudes of the negative biases are much reduced. On the other hand, the positive biases at mid- and high latitudes are enhanced. For ENSMEAN, the discrepancies from MILA-GPV are considerably smaller than those for WOA, EN3v2a and ARMOR3D for each of the criteria. The change in vertical resolution of profiles can be an error source as well as averaging of profiles as indicated by de Boyer Montégut et al. (2004). How these errors differ according to the criterion values is also an important question. In addition, representation of the interannual variability is relevant for climate studies as well as the climatology. These are quantitatively analyzed in the following subsections.

3.1 Errors due to averaging of profiles

de Boyer Montégut et al. (2004) previously revealed that averaging of profiles can lead to underestimations of MLD (shallower biases). In this subsection, we investigate the influence of

217 the time average by comparing the MLD/ILD estimates from monthly mean ("m") and
218 instantaneous ("i") TS profiles ("MLDr003m" and "MLDr003i" and likewise). Since both of the
219 above TS profiles are now provided by the MOVE-G2 experiment, our comparison here focuses
220 on the influence of the time average of profiles. In addition, interannually averaged monthly TS
221 profiles (like climatologies) are also used to estimate the MLDs/ILDs.
222
223 Underestimations in the zonal mean of greater than 10 m are seen in case of the monthly mean
224 profiles at mid-high latitudes in March-May (September-December) in the Northern (Southern)
225 Hemisphere (Fig. 2a, b). These are attributed to the re-stratification process of deep wintertime
226 MLDs/ILDs in the Kuroshio Extension region, in the south of the North Atlantic Current and in
227 the Southern Ocean and are generally 10-20 m (Fig. 2c, d). Note that larger biases can be seen
228 in the sea ice region. In addition, use of the climatological profiles (averaged over the 2001-
229 2011 period) results in further underestimation of MLD, especially in the tropics, where TS
230 profiles vary greatly in association with El Nino and Southern Oscillation (not shown).
231
232 In the latitudes of 20º-30º, underestimations from this effect are enlarged in March (September)
233 in the Northern (Southern) Hemisphere (e.g., Fig. 2a). A previous study (Takeuchi and Yasuda
234 2003) identified the MLD shoaling from February to March (from August to September) in a
235 large part of this latitude band in the Northern (Southern) Hemisphere, despite the fact that
236 monthly mean net surface heat flux is cooling the ocean surface. Since they used the averaged
237 profiles (e.g., WOA 1998), the MLD shoaling may partially be explained by the above
238 underestimations brought about by monthly averaging. Note that Takeuchi (2006) discussed the
239 possible effect of variability of surface heat flux within a month by using a simple ML model.
240

241 Similar effects can be expected from averaging of profiles over time as above and within a grid
242 cell, when the length scale calculated from the typical advection speed (e.g., 1 cm s^{-1} ×
243 1 month~26 km) is comparable to the grid spacing. Hence the above estimation for the effect
244 of averaging over time by using the MOVE-G2 result might be different from that for the effect
245 of averaging within a grid cell. In addition, the impact of temporal averaging of profiles in the
246 estimation of monthly MLD/ILD may be affected by the amount of high frequency variability,
247 which in turn may be affected by horizontal resolution. To address this question we have used
248 G2V3 which has a finer horizontal resolution (1/4º) than MOVE-G2 (1º zonally and 0.3-0.5º
249 meridionally). MLD/ILD estimates from monthly and daily mean TS profiles for an older
250 version of G2V3 have been compared. This comparison generally supports the above-described
251 underestimations of 10-20 m in early spring (not shown). Note that both reanalyses (MOVE-G2
252 and G2V3) assimilated the satellite-derived SLA observations (Table 2).
253
254 It should be noted that profiles from the real observations would have further variability on
255 smaller scales, which cannot be resolved in OGCMs. The averaging of these profiles may cause
256 the underestimation of MLD in the same way as indicated by de Boyer Montégut et al. (2004).
257 Therefore, the broad tendency of larger MLDs in ENSMEAN than in the observation-only
258 analyses as shown in Fig. 1 can be attributed to this effect partly.
259
260 Horizontal resolution can affect not only representation of the eddy-scale variability as
261 discussed above but also averaging area of TS profiles for the MLD/ILD estimation. In order to
262 investigate the latter effect, we compare the MLDs (MLDr003m and MLDr0125m) estimated
263 from monthly TS profiles in the MOVE-G2 experiment. Three TS profiles on the one-degree
264 resolution grids are used for the MLD estimation: 1) those interpolated from the MOVE-G2

grids (e.g., "MLDr003m_1x1"), 2) those smoothed by a 9-point filter after the interpolation (e.g., "MLDr003m_3x3") and 3) those smoothed by a 25-point filter after the interpolation (e.g., "MLDr003m_5x5"). Note that the smoothed profiles correspond to the profiles from low resolution analysis. As shown in Fig. 3, shallower MLDs are estimated when the smoothed (low resolution) TS profiles are used. This effect appears mostly in winter, in contrast to the effect of the time averaging (early spring; Fig. 2). Larger-scale smoothing results in greater magnitude of shoaling for both MLDr003m and MLDr0125m. While errors resulting from the smoothing at high latitudes are larger with the larger criterion ($\Delta\rho$ =0.125 kg m^{-3}), errors at mid-latitudes are smaller with the larger criterion. Although various resolutions (about 1/4-1º) are adopted for the reanalyses in this study, a tendency of shallower MLDs for reanalyses with lower resolutions is not seen as shown later (Section 4). Therefore, while horizontal resolution finer than 1º seems not to much influence the MLD estimation, the coarser resolutions (such as 3º and 5º) can largely affect the estimation.

3.2 Effect of vertical resolution

The average vertical resolutions of the observational profiles are 8.2 m, 2.3 m, 19.5 m and 9.4 m for profiling floats, CTD (Conductivity-Temperature-Depth), XBT (eXpendable BathyThermograph) and MBT (Mechanical BathyThermograph) measurements, respectively (de Boyer Montégut et al. 2004), whereas those for mooring arrays are usually about 20 m. On the other hand, the vertical resolutions of TS profiles in the syntheses can be much lower as shown in Fig. 4. For example, the vertical resolution of the WOA data is 25 (50) m at 50-150 (150-300) m depth. The low resolution of TS profiles can also be an error source in the MLD estimation.

289

290 Figure 5 shows schematic illustrations for the MLD estimations from high and low resolution
291 profiles. In the high resolution case (Fig. 5a) and low resolution case (1) (Fig. 5b), the estimated
292 MLDs are comparable to the "real" MLD (from the common simultaneous profile). On the other
293 hand, in the low resolution case (2) (Fig. 5c), the estimated MLD is much shallower than the
294 real MLD. Thus, MLD can be underestimated by using a low resolution vertical discretization
295 depending on the relative position of grids to the real MLD. In order to quantitatively assess this
296 effect, we generalize the MLD estimation as in Fig. 5d. Since we assume that we have at least
297 one grid point in the thermocline, which should hold for the most of the regions and resolutions
298 we investigate here, this simplified model does not contain a low-stratified layer beneath the
299 seasonal thermocline. We note that if the thermocline is not resolved with at least one grid point
300 overestimation of MLD can also happen. In fact, larger MLDs are estimated from the averaged
301 profiles than from the individual profiles, in particular with larger criteria, at high latitudes in
302 winter. There, the averaging of the profiles with a relatively weak thermocline results in a weak
303 thermocline being represented in the syntheses, leading to an overestimation of MLD/ILD, as
304 indicated by Noh and Lee (2008).
305

306 Here, the estimation error, *e*, is determined by using level spacing, Δz, relative position of the
307 bending point of the profile to the grid, *r*, and vertical density gradient of the seasonal
308 thermocline, $\frac{\partial \rho}{\partial z}$, as

309
$$e = \begin{cases} \Delta z(1-r) \times \frac{\frac{\partial \rho}{\partial z}\cdot\Delta z\cdot r - \Delta\rho}{\frac{\partial \rho}{\partial z}\cdot\Delta z\cdot r} & \text{for } c \equiv \frac{\Delta\rho}{\Delta z}\Big/\frac{\partial \rho}{\partial z} < r < 1 \\ 0 & \text{for } 1 < r < 1 + c \end{cases} \quad (1)$$

310 where *c* is the lower limit of *r*, and is given by the relation that the density at a grid point is

311 larger than the reference (10-m) value by $\Delta\rho$ exactly. (Although the true MLD would be the
312 bending point for this profile, we use the "real MLD" based on the density criterion here
313 considering the practical use with rather noisy profiles.) The expected error is then estimated as

314 $$\bar{e} = \int_c^{1+c} e dr \quad (2)$$

315 Figure 6 exhibits the expected error values depending on the vertical resolution for $\Delta\rho = 0.03$
316 and 0.125 kg m^{-3}, where Δz of 10 m corresponds to the vertical resolution of typical
317 observations. For $\Delta\rho = 0.03$ kg m^{-3}, the shallower errors at low- and mid-latitudes are within
318 5-7 (14-18) m with $\Delta z = 25$ (50) m (Fig. 6a). In case of $\Delta\rho = 0.125$ kg m^{-3}, the errors are
319 much smaller (e.g., 3-5 m with $\Delta z = 25$ m) and errors for the observational profiles are less
320 than 1 m (Fig. 6b). In contrast to the errors indicated in subsection 3.1, the distribution of the
321 errors from vertical resolution is rather broad in terms of time and space (e.g., Fig. 6c).
322
323 The mean differences of EN3v2a/ARMOR3D from MILA-GPV (over 40ºS-50ºN and the 2001-
324 2011 period) are -11.4 and -8.2 m for $\Delta\rho = 0.03$ and 0.125 kg m^{-3}, respectively. These
325 values are between the above estimations with $\Delta z = 25$ and 50 m (blue and red lines
326 respectively in Fig. 6a, b) and generally consistent with the resolutions of these data at the 100-
327 300 m depth (Fig. 4). Note that the Δz values vary with depth (and per dataset) and also that
328 use of vertical covariances of background errors (or smoothing) in the analyses can make the
329 resolution of the represented vertical variability coarser than the level spacing.
330
331 Differences between ENSMEAN and MILA-GPV are generally smaller than differences
332 between EN3v2a/ARMOR3D and MILA-GPV (Fig. 1) as described above. This can be largely
333 attributed to the higher vertical resolutions in the reanalyses, although the possible effect of
334 small scale variability in the real observation data might cause the shallower MLDs in the

observation-only analyses partly (subsection 3.1). Figure 4 represents the vertical resolution for each depth and synthesis. The level spacing of the reanalyses is generally less than 20 m at depths important for the ML variation (approximately the upper 200 m), which works well for the relatively small errors in the MLD and ILD fields of ENSMEAN. Note that relatively large ensemble size in this study should contribute to the generally small model errors in ENSMEAN.

3.3 Overestimation of ILDs in the subpolar regions

In addition to the aforementioned underestimations relative to MILA-GPV, overestimation of wintertime ILDs (biased-deep) estimated from the monthly mean TS profiles are seen in the subpolar regions. Figure 7 shows the ILDt05 distributions in March for MILA-GPV, WOA, EN3v2a and ARMOR3D. ILDs deeper than 400 m can be widely seen in the subarctic North Pacific in WOA, EN3v2a and ARMOR3D, while are only seen at a few grid points in MILA-GPV. Similar overestimation occurs in the Southern Ocean in austral winter (not shown).

In these subpolar regions, stratification is mostly determined by the halocline (e.g., Yuan and Talley 1996) and the thermocline is weak especially in winter (e.g., Dodimead 1967). A surface isothermal layer extending to the mesothermal layer (intermediate warm layer) can appear when the dicothermal structure (intermediate cold profile) weakens seasonally as shown, for example, in Fig. 8. However, since temperature in the surface layer changes rather rapidly if resolved with enough temporal resolution, this occurs only during a short period (Fig. 8a). On the other hand, the monthly data represent the occurrence of thick isothermal layer in a whole month, resulting in the overestimation greater than 100 m (Fig. 8b).

3.4 Interannual variability

A comprehensive assessment of the interannual anomaly field on a global scale is rather difficult due to limited independent observations. In this study, we assume white noise for the interannual anomaly field in each of the datasets and thereby investigate correlations of interannual signals between the datasets. Figure 9 presents the zonal mean correlation coefficients for interannual anomaly components in the data rich Argo period, using monthly data (seasonal cycle removed) for 2005-2011, among MILA-GPV, EN3v2a and ARMOR3D. Correlation coefficients (for MLDs in particular) are small at high latitudes presumably due to the limited number of observations there. At low- and mid-latitudes (about 50^{O}S-60^{O}N), values for MLDr003 and ILDt02 generally locate between 0.15 and 0.4 (Fig. 9a, b), whereas those for MLDr0125 and ILDt05 between 0.3 and 0.6 (Fig. 9c, d). Thus the interannual signals are more consistently represented when using the larger criteria ($\Delta\rho = 0.125$ kg m^{-3} and $\Delta T = 0.5^{O}$C).

In addition, correlation coefficients between EN3v2a and ARMOR3D (red) are larger than those between MILA-GPV and EN3v2a/ARMOR3D (light blue/light green) for MLDr0125 and ILDt05 (Fig. 9c, d). This suggests that the signal-to-noise ratio of the interannual anomalies are relatively low in MILA-GPV possibly due to the limited coverage by Argo floats. The correlation coefficients for MLDr0125 between EN3v2a and ARMOR3D (red) are lower by 0.1-0.2 at low latitudes than at mid-latitudes. This reduction of the correlation at low latitudes does not occur for ILDt05. This result implies that salinity analysis in the tropics may not be well constrained by observations. In fact, the lower correlation for MLDr0125 at low latitudes mainly results from relatively low correlation in the western Pacific warm pool region and in the Intertropical Convergence Zone (not shown), where salinity plays an important role in

383 determining the surface-layer stratification due to large freshwater input to the ocean. Note that,
384 although Shi et al. (An assessment of upper ocean salinity content from the Ocean Reanalyses
385 Inter-comparison Project (ORA-IP), submitted to the same issue of Climate Dynamics, 2015)
386 show that the averaged salinities over the 0-700 m depth in this region (156ºE, 8ºN) from the
387 reanalyses are generally consistent with the observations by the TRITON buoy, our result
388 indicates that the vertical salinity distribution in the upper ocean is still uncertain. Figure 10
389 compares the MLD/ILD time series in the western Pacific warm pool region (150ºE-180º, 5ºS-
390 5ºN). It is demonstrated that MLDr0125 time series (Fig. 10a) are much less consistent with
391 each other than the ILDt05 time series (Fig. 10b), the latter of which are well constrained by
392 relatively rich observations for temperature profiles by mooring arrays in the tropics. Variability
393 in MLDr0125 of ARMOR3D (green line) is relatively weak on both the seasonal and
394 interannual time scales. Although grid-scale correlation between MILA-GPV and EN3v2a is
395 rather lower (Fig. 9c), the area-mean values exhibit similar interannual variations, especially for
396 the period of the correlation analysis (2005-2011).
397
398 Zonal mean correlation coefficients between ENSMEAN and other datasets are shown in Fig.
399 9e, f. For both MLDr0125 and ILDt05, correlation coefficients between ENSMEAN and
400 EN3v2a/ARMOR3D (blue/green) are greater than those between ENSMEAN and MILA-GPV
401 (yellow) at low- and mid-latitudes. This fact also suggests relatively low signal-to-noise ratio of
402 the interannual variability in MILA-GPV as described above. Note that distortion of the
403 monthly MLD distributions by Argo sampling was reported in previous studies (e.g., Juza et al.
404 2012). On the other hand, the variability in MILA-GPV is by and large consistent with the
405 variability in ENSMEAN in terms of area-mean values, especially for the 2005-2011 period
406 (e.g., Fig. 10).

Correlation coefficients between ENSMEAN and EN3v2a/ARMOR3D (blue/green) are generally greater than those between EN3v2a and ARMOR3D (red) as shown in Fig. 9e, f. This suggests better representation of interannual signals in ENSMEAN, which can be attributed to the use of atmospheric information as surface forcing. Independent validations will ensure the effectiveness of the ensemble use of reanalyses in detecting interannual variability, which awaits future work.

4 Intercomparison of the reanalysis MLDs/ILDs

4.1 Seasonal and interannual variations of MLDs

Seasonal variations of MLDs are basically characterized by the winter- and summer-time MLD features. Following the discussion in subsection 3.1, MLDs in February and August are compared among the syntheses as typical of MLDs in winter and summer respectively with relatively small errors (e.g., MLDs in March are considered to have larger errors). Figures 11 and 12 show that the MLDr0125 discrepancies from MILA-GPV are relatively large in the winter hemisphere on a basin scale for both the observation-only analyses and reanalyses. Distributions for MLDr003, ILDt02 and ILDt05 (figures not shown) are generally similar to those for MLDr0125.

In February (Fig. 11), positive discrepancies are seen in the Kuroshio Extension and recirculation regions in most of the reanalyses, where common biases are known in coarse

resolution models (e.g., Hasumi et al. 2010). Similar positive discrepancies are exhibited in the Gulf Stream recirculation region. Positive discrepancies can also be seen in the Arabian Sea and Bay of Bengal for all the renalyses except G2V3 and ECCO-v4. In addition, in many reanalyses, negative discrepancies are seen in the Southern Ocean (in austral summer) such as reported in several studies (e.g., Gnanadesikan et al. 2006; Noh and Lee 2008). Note that MLDs become larger from ORAS4 to ORAP5 in this region probably by incorporating the effects of the wave breaking and Langmuir circulation (Janssen 2012), although other updates of the system (e.g., horizontal resolution) may also have a contribution. Since the above discrepancies are not seen in the observation-only analyses (EN3v2a and ARMOR3D), these can be considered as weakness of the reanalyses that need to be improved.

Negative discrepancies from MILA-GPV are predominant in the North Atlantic Current region for many syntheses including the observation-only analyses. These can be attributed to overestimations of the monthly MLDs by Argo sampling in winter in this region (up to about 50 m) indicated by Juza et al. (2012) at least partly. It is considered that, in the subpolar North Atlantic, both limited observations and poor representations by models affect the large ensemble spread of the syntheses which is defined in this study as the standard deviation from the ensemble mean (e.g., Xue et al. 2012). However, since the absolute MLD values are several times larger in this region than in other regions, normalized ensemble spread values larger than 0.4 generally occur in limited regions near the coast.

Weak negative discrepancies in the tropics for all the syntheses are consistent with our results described in subsection 3.2. Although negative discrepancies in the subarctic North Pacific for ENSMEAN are comparable to those for EN3v2a and ARMOR3D, their amplitudes for the

individual reanalyses differ greatly: negative discrepancies larger than the ENSMEAN values in G2V3, GECCO2, ECCO-NRT, ECDA, K7-ODA, K7-CDA, MOVE-G2 and MOVE-CORE; positive discrepancies in C-GLORS, UR025.4 and GloSea5. The overall patterns are similar in C-GLORS, UR025.4 and GloSea5, suggesting that, in this cluster, the choice of model (NEMO3.2), forcing (ERA-interim (ERAi)) and resolution (Table 2) plays a dominant role in determining the MLD. Note that horizontal resolution often influences the tuning of parameterizations such as isopycnal diffusivity that is important to the representation of the stratification in the subpolar regions. Although G2V3, ORAS4 and ORAP5 also use the NEMO model and ERA-interim forcing, a bias correction scheme (Balmaseda et al. 2007) might work to reduce the above positive biases. Note that, although the ERA-interim forcing is also used for ECCO-v4, it is corrected through the 4DVAR approach. Another cluster includes MERRA, ECDA and PEODAS, which commonly use the MOM models and also show similar patterns. Although K7-ODA and K7-CDA also use the MOM3, the assimilation method they use (4DVAR) appears to have stronger effect on the MLD patterns.

In August (Fig. 12), the large MLDs around the Antarctic Circumpolar Current (ACC) region as represented in MILA-GPV are estimated to be smaller in most of the reanalyses. In addition, the amplitudes of the discrepancies are remarkably different between the datasets, and hence the ensemble spread in this region is relatively large. Improvement in representing MLDs in this region is needed in the future. To do so, intercomparisons for sea ice (e.g., Smith et al. 2014) and surface flux (e.g., Valdivieso et al. 2014) might indicate important clues in association with deep convection following the sea ice formation by strong cooling. Further observations in the Southern Ocean, particularly for the sea ice region, are also important, indicated by large differences between MILA-GPV and EN3v2a/ARMOR3D with their signs changing on small

479 scales.

480

481 Positive discrepancies in the mid-latitude South Pacific and Atlantic seen in C-GLORS,
482 UR025.4 and GloSea5 (Fig. 12) are similar to those in the North Pacific in boreal winter (Fig.
483 11). In the South Indian Ocean, positive discrepancies are also seen in most of the reanalyses,
484 which can be attributed partly to a weak representation of the Agulhas retroflection in coarse
485 resolution models as reported by previous studies (e.g., Morioka et al. 2012). Such difficulty in
486 representing the MLD variability is also seen in several reanalyses in the confluent region
487 between the Brazil and Malvinas Currents. The above limitations are also found in the
488 intercomparison of the salinity fields (Alves et al. 2014).

489

490 Negative discrepancies in the western tropical Pacific are observed in several reanalyses.
491 Previous studies have reported that precipitation inputs derived from atmospheric reanalysis
492 datasets are much larger than satellite-based estimates in this region (Iwasaki et al. 2014). On
493 the other hand, evaporation for OGCMs is usually estimated from the bulk formula by using
494 simulated SST as in the reanalyses here. The model experiment using the above freshwater
495 fluxes often generates a too strong halocline, thereby leading to negative MLD biases.
496 Assimilation of the recent sea surface salinity observations from satellites is likely to reduce
497 these biases (e.g., Köhl et al. 2014, Toyoda et al. 2015). Furthermore, better results from the
498 reanalyses with ocean-atmosphere coupled models (ECDA and MOVE-C) suggest an advantage
499 of these approaches (e.g., Fujii et al. 2009) as they may eliminate some of the uncertainties
500 associated with precipitation forcing from atmospheric analysis. Obviously, further validation
501 studies for the freshwater fluxes reproduced or corrected in the reanalyses are necessary. This
502 would be addressed in the ORA-IP.

503

504 The skillful reproduction of the interannual variability in the ENSMEAN MLDr0125 field is
505 demonstrated in subsection 3.4. Here, we intercompare the correlation of the individual
506 reanalyses with ENSMEAN. Figure 13 shows the distributions of correlation coefficients for the
507 interannual anomalies of MLDr0125 between ENSMEAN and the individual
508 reanalyses/syntheses. Correlation is low at high latitudes as seen for the observation-only
509 analyses (Fig. 9e). At low and mid-latitudes, relatively large correlation can be seen in ORAS4
510 and MOVE-G2. Since both reanalyses use coarse resolution (about 1º) and the 3DVAR method,
511 higher resolution or sophisticated assimilation method does not always improve the
512 reproduction of the interannual variability. Relatively small correlation coefficients are seen in
513 the Kuroshio Extension, Gulf Stream, Agulhas retroflection and Malvinas Current regions,
514 where discrepancies in mean values from MILA-GPV are also large (Fig. 11, 12). In the regions
515 relevant to El Nino and Southern Oscillation and the Pacific decadal oscillation (e.g., Mochizuki
516 et al., 2010), the correlation coefficients are relatively large for most of the reanalyses, which
517 encourage possible applications of the reanalysis datasets to the studies on these oscillations.
518

519 For both observation-only analyses (bottom row in Fig. 13), correlation coefficients at mid-
520 latitudes are higher for MLDr0125 than for ILDt05, as seen in Fig. 9e, f, although these are
521 generally smaller than those between ENSMEAN and the reanalyses. As also seen in Fig. 9e,
522 the correlation coefficients for MLDr0125 are lower at low latitudes than at mid-latitudes. It is
523 shown in Fig. 13 that this arises from relatively low values in the regions of low surface salinity
524 (e.g., the Indonesian maritime continent and the region of the Amazon River plume). In
525 particular, the correlation for MLDr0125 between ENSMEAN and ARMOR3D is remarkably
526 low, consistent with the result shown in Fig. 10. Surface salinity observations from satellites

will possibly contribute to the improvements of the analyses in these regions (e.g., Toyoda et al., 2015). Also, observations by the mooring array are required to be maintained in order to keep or enhance the quality of the reanalyses/syntheses.

4.2 Barrier layer thicknesses

The barrier layer is the isothermal layer below the ML that prevents cooling of the ML by entrainment of the underlying waters (e.g., Lukas and Lindstrom 1991). Therefore, the barrier layer thickness (BLT), which is usually deduced from the MLD and ILD, is an important parameter for the surface heat budget in climate studies. In this subsection, BLTs from the syntheses are examined to evaluate the integrated reproduction of the MLDs and ILDs. BLT is defined in this study as difference between MLDr0125 and ILDt05 only when ILDt05 is larger than MLDr0125 (e.g., Maes et al. 2006).

Figure 14 shows the distributions of the BLTs from the syntheses. Results are only displayed for low- and mid-latitudes because of the issues with ILDs at high latitudes (subsection 3.3). Large BLTs present in the western equatorial Pacific and Atlantic and the north-eastern Indian Ocean are represented in MILA-GPV, EN3v2a and ARMOR3D. BLTs in the western Pacific and eastern Indian Oceans are larger in EN3v2a and ARMOR3D than in MILA-GPV. In objective analyses, a large zonal correlation scale may be used owing to fast wave speeds in the tropics. On the other hand, a recent study using the Argo data that the barrier layer develops and ceases on a rather shorter time scale (Katsura and Oka 2014). This fact implies the presence of smaller-scale correlations there due to a confined distribution of intense BLTs as in MILA-GPV.

551 In addition to the formation of BLTs associated with excess precipitation (and also river
552 discharge) over evaporation in the tropics, another generating mechanism associated with
553 subduction of the salty subtropical waters can be seen around the boundaries between tropics
554 and subtropics. For example, pronounced BLTs around 10^{O}N -20^{O}N in the North Pacific are
555 thought to come from both the North Pacific tropical water (e.g., Suga et al. 2000) and eastern
556 subtropical mode water (e.g., Toyoda et al. 2004). These BLTs are greater in ARMOR3D than in
557 MILA-GPV and EN3v2a in both North and South Pacific. This might result from the use of
558 vertical modes in synthesizing satellite data (e.g., SLA and SST) as well as in-situ TS profiles in
559 ARMOR3D (Table 1).
560
561 The reanalyses basically reproduce the above features of the BLT distribution seen in the
562 observational datasets. For example, the important aspects of BLTs in the western tropical
563 Pacific are well represented in ENSMEAN, comparable to MILA-GPV in a quantitative sense.
564 Note that BLTs are relatively small in GECCO2, ECCO-NRT and K7-ODA, which all use the
565 smoother approaches (e.g., 4DVAR and KS). This suggests that the control of the salinity field
566 (such as by adjusting the surface freshwater fluxes) is still challenging in the smoother
567 approach. In contrast, BLTs in the coupled reanalyses (ECDA, K7-CDA and MOVE-C) are
568 quantitatively comparable to those in MILA-GPV and ENSMEAN, which is encouraging for
569 the use of coupled models.
570
571
572 **5 Summary and discussion**
573
574 In the present study, we have investigated the fidelity of a suite of global ocean synthesis

products in representing the MLD/ILD fields which are recognized as an important element in the ocean circulation system. These syntheses, including 2 observation-only analyses and 17 reanalyses which assimilate data into models, have been provided by operational and research centers as an international action of the ORA-IP (Balmaseda et al. 2014). First, we compared the observation-only analyses with reference datasets (de Boyer Montégut et al. 2004; Hosoda et al. 2010) that determined MLD directly from individual TS profiles. The purpose is to investigate the errors in estimating MLDs/ILDs unrelated to model errors. Negative biases are seen in the MLDs/ILDs from monthly mean and gridded TS profiles of the above syntheses with respect to those from individual profiles as reported by de Boyer Montégut et al. (2004). It is revealed that these underestimations from the averaging procedure of profiles are associated with a rapid re-stratification process to the relatively deep ML state in early spring and estimated to be approximately 10-20 m. In addition, negative biases are generated depending on the vertical resolutions of profiles, which are distributed more broadly in time and space. When the criterion $\Delta\rho = 0.03$ kg m^{-3} is used, the underestimations from this effect are estimated as 5-7 (14-16) m for the vertical resolution $\Delta z = 25$ (50) m. On the other hand, they are generally much smaller in case of the larger criterion $\Delta\rho = 0.125$ kg m^{-3}. Furthermore, considerable overestimations (greater than 100 m) of the wintertime ILDs from the monthly mean profiles are seen in subpolar regions in association with the mesothermal structure.

Discrepancies between the ensemble mean obtained from the 17 sets of reanalyses and the reference datasets are noticeably smaller than the observation-only analyses in many regions where model errors in the individual reanalyses are mutually canceled out through the ensemble averaging approach. This can be attributed mainly to the higher vertical resolutions of the reanalyses in reproducing the MLDs as well as the large ensemble size. The results (e.g., Fig. 1)

599 show, on the other hand, that there exist a few regions where model errors are not canceled by
600 the ensemble mean (such as the Kuroshio Extension and ACC regions). Such common model
601 errors possibly arise from the coarse horizontal resolutions as reported in previous studies (e.g.,
602 Hasumi et al. 2010). Interannual variability is better represented in both the analyses using all
603 available TS observations (including Argo data) and the ensemble mean of the reanalyses than
604 the analysis using the Argo data only, especially when the larger values are used for the criteria
605 ($\Delta\rho = 0.125$ kg m^{-3} and $\Delta T = 0.5^{o}$C).
606
607 Differences in the individual syntheses were then assessed by intercomparing the winter and
608 summer MLDs/ILDs together with the BLTs. The result shows that, in addition to the consistent
609 features between the reanalyses, differences can also be seen depending on the configurations of
610 the reanalyses. Features seen in the reanalyses with similar configurations offer interesting
611 information toward the improved reanalyses (e.g., the change in mixing parameterization from
612 ORAS4 to ORAP5) and also suggests a limit to the effectiveness of the ensemble mean
613 approach if similar reanalyses are included. At high latitudes, consistency among all the
614 observational and reanalysis datasets is relatively low in terms of both the seasonal cycle and
615 interannual variability. Therefore, observational studies that fully describe the high-latitudinal
616 variability are required as well as further improved modeling and assimilation techniques
617 toward the enhanced syntheses.
618
619 Although MLD/ILD data themselves are not assimilated in the syntheses here, the estimated
620 MLDs/ILDs are primarily influenced by the assimilated TS profile data. Therefore, regarding
621 the observational MLDs/ILDs as independent references might yield little extra effect. In
622 addition, smaller biases in a product do not necessarily indicate its superiority in other aspects.

623 Their magnitude depends on how strongly the observations of TS are used to constrain the
624 model locally in time and space. For example, the smoother approach does not insert local TS
625 corrections but tends to retain the model dynamics while trying to fit the model to the data,
626 which makes an MLD representation close to the observational data rather challenging. Hence,
627 it is important to make an accurate assessment of each synthesis from various aspects,
628 particularly with independent data. However, taking into consideration the fact that the MLD is
629 a key parameter in determining the upper ocean processes, which greatly influences other
630 variables, the validation and intercomparison of the MLD fields of the syntheses in this study
631 are of value for the communities of both model developers and users. In particular, the robust
632 reproduction of both the seasonal cycle and interannual variability of MLD by the ensemble
633 mean of the renalyses indicates a great potential of the ensemble mean MLD field for better
634 investigating and monitoring the upper ocean processes, together with other intercomparison
635 results such as for the surface forcing and heat content variability (e.g., Palmer et al. 2014).
636 Information on uncertainty derived from the ensemble spread should allow further quantitative
637 discussion for results derived from the ensemble mean (e.g., Xue et al. 2012).
638
639
640 **Acknowledgements**
641
642 We thank two anonymous reviewers for their constructive comments. The MILA-GPV dataset
643 (Hosoda et al. 2010) is provided by the RCGC/JAMSTEC from their web site at
644 http://www.jamstec.go.jp/ARGO/argo_web/MILAGPV/. The MLD dataset of de Boyer
645 Montégut et al. (2004) is obtained from his web site at
646 http://www.ifremer.fr/cerweb/deboyer/mld/home.php. The Argo float data are provided by the

NODC/NOAA at their web site http://www.nodc.noaa.gov/OC5/WOD13/. This work was partly supported by the Research Program on Climate Change Adaptation (RECCA) of the Ministry of Education, Culture, Sports, Science and Technology of the Japanese government (MEXT), by the Data Integration and Analysis System (DIAS) of the MEXT, by the joint UK DECC/Defra Met Office Hadley Centre Climate Programme (GA01101), by the UK Public Weather Service Research Programme, and by the European Commission funded projects MyOcean (FP7-SPACE-2007-1) and MyOcean2 (FP7-SPACE-2011-1). During the preparation of this article, our co-author Nicolas Ferry passed away. He was an active and supportive member of the ORA-IP and CLIVAR-GSOP activities.

References

Alves O, Shi L, Wedd R, Balmaseda M, Chang Y, Chepurin G, Fujii Y, Gaillard F, Good S, Guinehut S, Haines K, Hernandez F, Lee T, Palmer M, Peterson KA, Masuda S, Storto A, Toyoda T, Valdivieso M, Vernieres G, Wang X, Yin Y (2014) An assessment of upper ocean salinity reanalyses from CLIVAR GSOP/GODAE system. CLIVAR EXCHANGES 64:11-14

Balmaseda MA, Dee D, Vidard A, Anderson DLT (2007) A multivariate treatment of bias for sequential data assimilation: application to the tropical oceans. QJR Meteorol Soc 133:167–179. doi:10.1002/qj.12

Balmaseda MA, Hernandez F, Storto A, Palmer MD, Alves O, Shi L, Smith GC, Toyoda T, Valdivieso M, Barnier B, Behringer D, Boyer T, Chang YS, Chepurin GA, Ferry N, Forget G, Fujii Y, Good S, Guinehut S, Haines K, Ishikawa Y, Keeley S, Köhl A, Lee T, Martin M, Masina

672 S, Masuda S, Meyssignac B, Mogensen K, Parent L, Peterson KA, Tang YM, Yin Y, Vernieres
673 G, Wang X, Waters J, Wedd R, Wang O, Xue Y, Chevallier M, Lemieux JF, Dupont F, Kuragano
674 T, Kamachi M, Awaji T, Caltabiano A, Wilmer-Becker K, Gaillard F (2015) The Ocean
675 Reanalyses Intercomparison Project (ORA-IP). J Operational Oceanogr (in press).
676 doi:10.1080/1755876X.2015.1022329
677
678 Blanke B, Delecluse P (1993) Variability of the tropical Atlantic ocean simulated by a general
679 circulation model with two different mixed-layer physics. J Phys Oceanogr 23:1363-1388
680
681 Chang YS, Zhang S, Rosati A, Delworth TL, Stern WF (2013) An assessment of oceanic
682 variability for 1960–2010 from the GFDL ensemble coupled data assimilation. Clim
683 Dyn 40:775-803. doi:10.1007/s00382-012-1412-2
684
685 Chen D, Busalacchi AJ, Rothstein LM (1994) The roles of vertical mixing, solar-radiation, and
686 wind stress in a model simulation of the sea-surface temperature seasonal cycle in the tropical
687 Pacific-Ocean. J Geophys Res 99(C10):20345-20359
688
689 Danabasoglu G, co-authors (2014) North Atlantic simulations in coordinated ocean-ice
690 reference experiments phase II (CORE-II). Part I: Mean state. Ocean Modell 73:76-107.
691 doi:10.1016/j.ocemod.2013.10.005
692
693 de Boyer Montégut C, Madec G, Fischer AS, Lazar A, Iudicone D (2004) Mixed layer depth
694 over the global ocean: An examination of profile data and a profile-based climatology. J
695 Geophys Res 109:C12003. doi:10.1029/2004JC002378

696

697 Dodimead AJ (1967) Winter oceanographic conditions in the Central Subarctic Pacific. Int
698 North Pacific Comm 999:1-14

699

700 Ferry N, Parent L, Garric G, Bricaud C, Testut CE, Le Galloudec O, Lellouche JM, Drévillon
701 M, Greiner E, Barnier B, Molines JM, Jourdain N, Guinehut S, Zawadzki L (2012)
702 GLORYS2V1 global ocean reanalysis of the altimetric era (1993-2009) at meso scale. Mercator
703 Ocean Newsletter 44:28-39.

704

705 Fujii, Y, Nakaegawa N, Matsumoto S, Yasuda T, Yamanaka G, Kamachi M (2009) Coupled
706 climate simulation by constraining ocean fields in a coupled model with ocean data. J Clim
707 22:5541-5557

708

709 Gnanadesikan A et al. (2006) GFDL's CM2 global coupled climate models. Part II: The baseline
710 ocean simulation. J Clim 19:675-697. doi:10.1175/JCLI3630.1

711

712 Guinehut S, Dhomps AL, Larnicol G, Le Traon PY (2012) High resolution 3D temperature and
713 salinity fields derived from in situ and satellite observations. Ocean Sci 8:845-857.
714 doi:10.5194/os-8-845-2012

715

716 Hosoda S, Ohira T, Sato K, Suga T (2010) Improved description of global mixed-865 layer
717 depth using Argo profiling floats. J Oceanogr 66:773-787. doi:10.1007/s10872-866 010-0063-3

718

719 Ingleby B, Huddleston M (2007) Quality control of ocean temperature and salinity profiles -

720 historical and real-time data. Journal of Marine Systems 65:158-175.
721 doi:10.1016/j.jmarsys.2005.11.019
722
723 Iwasaki S, Kubota M, Watabe T (2014) Assessment of various global freshwater flux products
724 for the global ice-free oceans. Rem Sens Env, 140:549-561. doi:10.1016/j.rse.2013.09.026.
725
726 Janssen PAEM (2012) Ocean wave effects on the daily cycle in SST. J Geophys Res
727 117:C00J32. doi:10.1029/2012JC007943
728
729 Juza M, Penduff T, Brankart JM, Barnier B (2012) Estimating the distortion of mixed layer
730 property distributions induced by the Argo sampling. J Oper Oceanogr 5:45-58.
731
732 Katsura S, Oka E (2014) Formation mechanism of winter barrier layer in the subtropical Pacific.
733 2014 Ocean Science Meeting, 23-28 February 2014, Honolulu Hawaii USA
734
735 Köhl A (2014) Evaluation of the GECCO2 ocean synthesis: transports of volume, heat and
736 freshwater in the Atlantic. QJR Meteorol Soc. doi:10.1002/qj.2347
737
738 Köhl A, Sena Martins M, Stammer D (2014) Impact of assimilating surface salinity from SMOS
739 on ocean circulation estimates. J Geophys Res 119:5449-5464. doi:10.1002/2014JC010040
740
741 Lahoz W, Errera Q (2010) Constituent assimilation. In: Lahoz W, Khattatov B, Menard R (ed)
742 Data Assimilation, Making Sense of Observations. Springer, New York, pp 449-490.
743 doi:10.1007/987-3-540-74703-1

744

745 Large WG, McWilliams JC, Doney SC (1994) Oceanic vertical mixing: A review and a model
746 with a nonlocal boundary layer parameterization. Rev Geophys 32:363-403

747

748 Lee T, Awaji T, Balmaseda MA, Grenier E, Stammer D (2009) Ocean state estimation for
749 climate research. Oceanography 22:160-167. doi:10.5670/oceanog.2009.74

750

751 Levitus S (1982) Climatological atlas of the world ocean. NOAA/ERL GFDL, Princeton NJ
752 USA, 173 pp

753

754 Locarnini RA, Mishonov AV, Antonov JI, Boyer TP, Garcia HE, Baranova OK, Zweng MM,
755 Johnson DR (2010) World Ocean Atlas 2009, Volume 1: Temperature. In: Levitus S (ed) NOAA
756 Atlas NESDIS 68, US Government Printing Office, Washington DC USA, pp 184

757

758 Lukas R, Lindstrom E (1991) The mixed layer of the western equatorial Pacific Ocean. J
759 Geophys Res 96:3343-3357

760

761 Maes C, Ando K, Delcroix T, Kessler WS, McPhaden MJ, Roemmich D (2006) Observed
762 correlation of surface salinity, temperature and barrier layer at the eastern edge of the western
763 Pacific warm pool. Geophys Res Lett 33:L06601. doi:10.1029/2005GL024772

764

765 Masuda S, Awaji T, Sugiura N, Matthews JP, Toyoda T, Kawai Y, Doi T, Kouketsu S. Igarashi
766 H, Katsumata K, Uchida H, Kawano T, Fukasawa M (2010) Simulated rapid warming of
767 abyssal North Pacific waters. Science 329:319-322. doi;10.1126/science.1188703

768

769 Mochizuki T, Ishii M, Kimoto M, Chikamoto Y, Watanabe M, Nozawa T, Sakamoro TT,
770 Shiogama H, Awaji T, Sugiura N, Toyoda T, Yasunaka S, Tatebe H, Mori M (2010) Pacific
771 decadal oscillation hindcasts relevant to near-term climate prediction. Proc Natl Acad Sci USA
772 107:1833-1837. doi:10.1073/pnas.0906531107

773

774 Morioka Y, Tozuka T, Masson S, Terray P, Luo JJ, Yamagata T (2012) Subtropical dipole modes
775 simulated in a coupled general circulation model. J Clim 25:4029-4047. doi:10.1175/JCLI-D-
776 11-00396.1

777

778 Noh Y, Kang YJ, Matsuura T, Iizuka S (2005) Effect of the Prandtl number in the
779 parameterization of vertical mixing in an OGCM of the tropical Pacific. Geophys Res Lett
780 32:L23609. doi:10.1029/2005GL024540

781

782 Noh Y, Lee WS (2008) Prediction of the mixed and mixing layer depths from an OGCM. J.
783 Oceanogr 64:217-225. doi:10.1007/s10872-008-0017-1

784

785 Pedlosky J (1996) Ocean circulation theory. Springer Berlin Heidelberg, 456 pp.
786 doi:10.1007/987-3-662-03204-6

787

788 Palmer M, Balmaseda M, Chang YS, Chepurin G, Fujii Y, Good S, Guinehut S, Hernandez F,
789 Martin M, Masuda S, Peterson KA, Toyoda T, Valdivieso M, Vernieres G, Wang O, Xue Y
790 (2014) GLIVAR-GSOP/GODAE intercomparison of ocean heat content: initial results. CLIVAR
791 EXCHANGES 64:8-10

792

793 Shay LK, Goni GJ, Black PG (2000) Effects of a warm oceanic feature on Hurricane Opal. Mon
794 Wea Rev 128:1366–1383

795

796 Smith G, Chevallier M, Lemieux JF, Dupont F, Vernieres G, Storto A, Toyoda T, Fujii Y,
797 Chang Y, Valdivieso M, Peterson KA, Ferry N, Hernandez F, Balmaseda MA, Keeley S, Wang
798 X (2014) Preliminary evaluation of sea ice fields form the ocean reanalyses intercomparison
799 project. CLIVAR EXCHANGES 64:32-34

800

801 Storto A, Dobricic S, Masina S, Di Pietro P (2011) Assimilating along-track altimetric
802 observations through local hydrostatic adjustment in a global ocean variational assimilation
803 system. Mon Wea Rev 139:738-754. doi:10.1175/2010MWR3350.1

804

805 Suga T, Kato A, Hanawa K (2000) North Pacific Tropical Water: its climatology and temporal
806 changes associated with the climate regime shift in the 1970s. Prog Oceanogr 47:223-256

807

808 Sugiura N, Awaji T, Masuda S, Mochizuki T, Toyoda T, Miyama T, Igarashi H, Ishikawa Y
809 (2008) Development of a four-dimensional variational coupled data assimilation system for
810 enhanced analysis and prediction of seasonal to interannual climate variations. J Geophys Res
811 113:C10017. doi:10.1029/2008JC004741

812

813 Takeuchi E (2006) Studies on the wintertime shoaling of oceanic surface mixed layer. PhD
814 thesis, University of Tokyo, 109 pp

815

816 Takeuchi E, Yasuda I (2003) Wintertime shoaling of oceanic surface mixed layer. Geophys Res
817 Lett 30:2152. doi:10.1029/2003GL018511
818
819 Toyoda T, Awaji T, Ishikawa Y, Nakamura T (2004) Preconditioning of winter mixed layer in
820 the formation of North Pacific eastern subtropical mode water. Geophys Res Lett 31:L17206.
821 doi:10.1029/2004GL020677
822
823 Toyoda T, Fujii Y, Kuragano T, Kamachi M, Ishikawa Y, Masuda S, Awaji T, Hernandez F,
824 Ferry N, Guinehut S, Martin M, Peterson KA, Good S, Valdivieso M, Haines K, Storto A, Köhl
825 A, Yin Y, Shi L, Smith G, Chang Y, Vernieres G, Wang X, Wang O, Lee T, Balmaseda M
826 (2014) Mixed layer depth intercomparison among global ocean syntheses reanalyses. CLIVAR
827 EXCHANGES 64:22-24
828
829 Toyoda T, Fujii Y, Kuragano T, Matthews JP, Abe H, Ebuchi N, Usui N, Ogawa K, Kamachi M
830 (2015) Improvements to a global ocean data assimilation system through the
831 incorporation of Aquarius surface salinity data. QJR Meteorol Soc (in press).
832 doi:10.1002/qj.2561
833
834 Toyoda T, Fujii Y, Yasuda T, Usui N, Iwao T, Kuragano T, Kamachi M (2013) Improved
835 analysis of the seasonal-interannual fields by a global ocean data assimilation system.
836 Theoretical and Applied Mechanics Japan 61: 31-48. doi:10.11345/nctam.61.31
837
838 Umlauf L, Burchard H (2003) A generic length-scale equation for geophysical turbulence
839 models. J Mar Res 61(2):235-265. doi:10.1357/002224003322005087

840

841 Valdivieso M, Haines K, Balmaseda M, Barnier B, Chang Y, Ferry N, Fujii Y, Köhl A, Lee T,
842 Martin M, Storto A, Toyoda T, Wang X, Waters J, Xue Y, Yin Y (2014) Heat fluxes from ocean
843 and coupled reanalyses. CLIVAR EXCHANGES 64:28-31

844

845 Vernieres G, Rienecker MM, Kovach R, Keppenne C (2012) The GEOS-iODAS: Description
846 and evaluation. NASA Tech Rep Series on Global Modeling and Data Assimilation 30:TM-
847 2012-104606, GSFC/NASA, Greenbelt Maryland USA

848

849 Yin Y, Alves O, Oke PR (2011) An ensemble ocean data assimilation system for seasonal
850 prediction. Mon Wea Rev 139:786-808. doi:10.1175/2010MWR3419.1

851

852 Yuan XJ, Talley LD (1996) The subarctic frontal zone in the North Pacific: Characteristics of
853 frontal structure from climatological data synoptic surveys. J Geophys Res 101:16491-16508

854

855 Xue Y, Balmaseda MA, Boyer T, Ferry N, Good S, Ishikawa I, Kumar A, Rienecker M, Rosati
856 AJ, Yin Y (2012) A comparative analysis of upper-ocean heat content variability from an
857 ensemble of operational ocean reanalyses. J Clim 25:6905-6929. dio:10.1175/JCLI-D-11-
858 00542.1

859

860 Zuo H, Balmaseda MA, Mogensen K (2014) The ECMWF-MyOcean2 eddy-permitting ocean
861 and sea-ice re-analysis ORAP5. Part 1: Implementation. Tech Rep 736, ECMWF, Reading UK

862

863

Figure captions

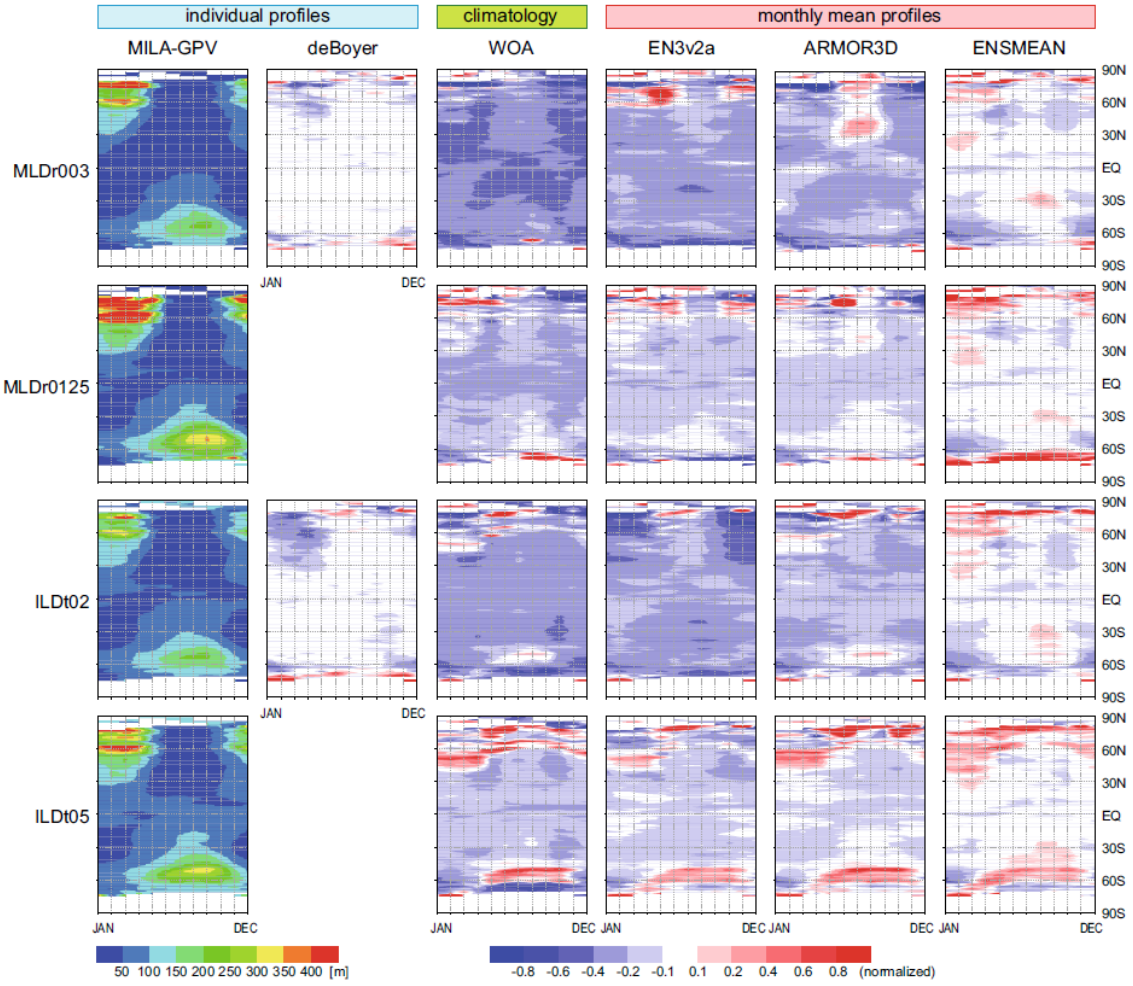

Fig. 1 Zonal mean monthly distributions of MLDr003, MLDr0125, ILDt02 and ILDt05 averaged over 2001-2011 for (left column) MILA-GPV and (others) differences from MILA-GPV, normalized by the MILA-GPV values.

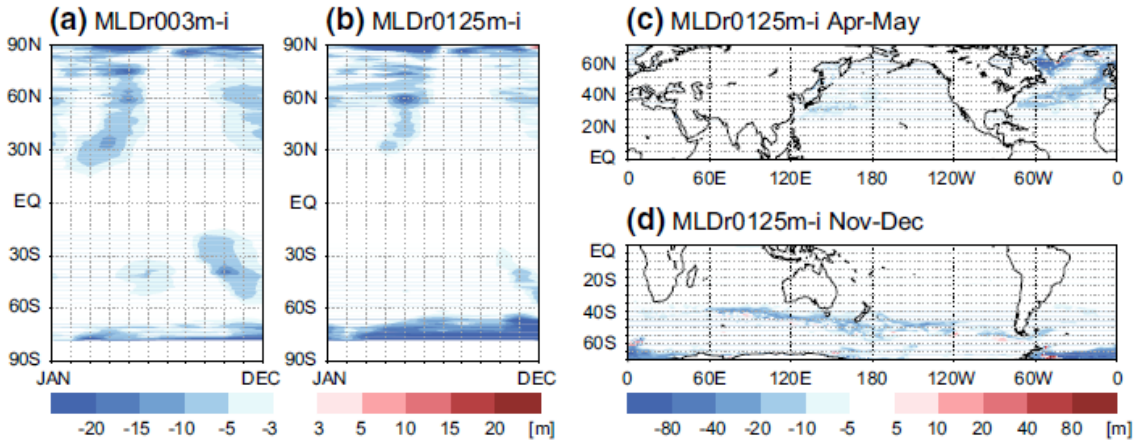

871

872 **Fig. 2** (a, b) Zonal mean monthly differences MLDr003m−MLDr003i (a) and

873 MLDr0125m−MLDr0125i (b) estimated from MOVE-G2 during the 2001-2012 period. (c, d)

874 Distributions of MLDr0125m−MLDr0125i in April-May (c) and November-December (d).

875

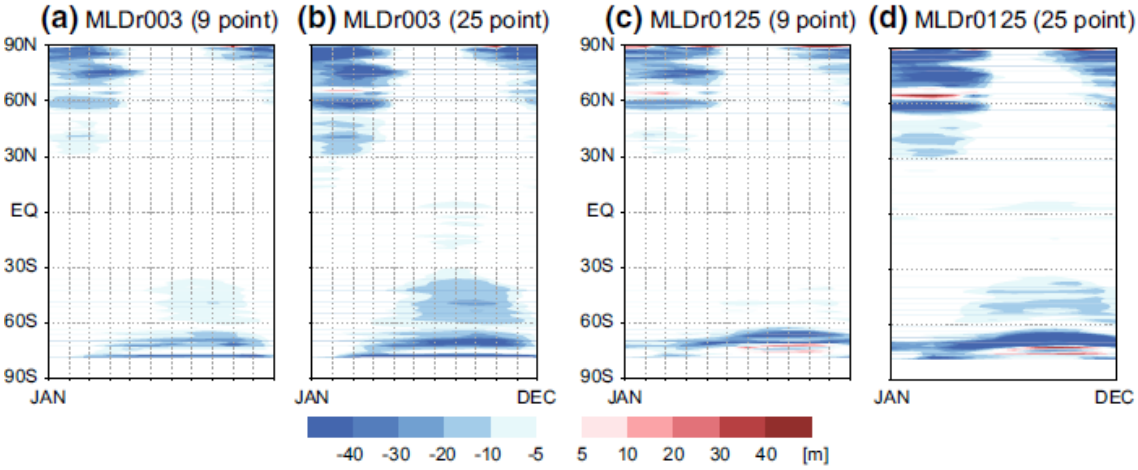

876

877 **Fig. 3** Zonal mean monthly differences between MLDs from smoothed and unsmoothed TS

878 profiles during the 2001-2012 period in the MOVE-G2 experiment. (a)

879 MLDr003m_3x3−MLDr003m_1x1. (b) MLDr003m_5x5−MLDr003m_1x1. (c, d) Same as (a,

880 b) but for MLDr0125m.

881

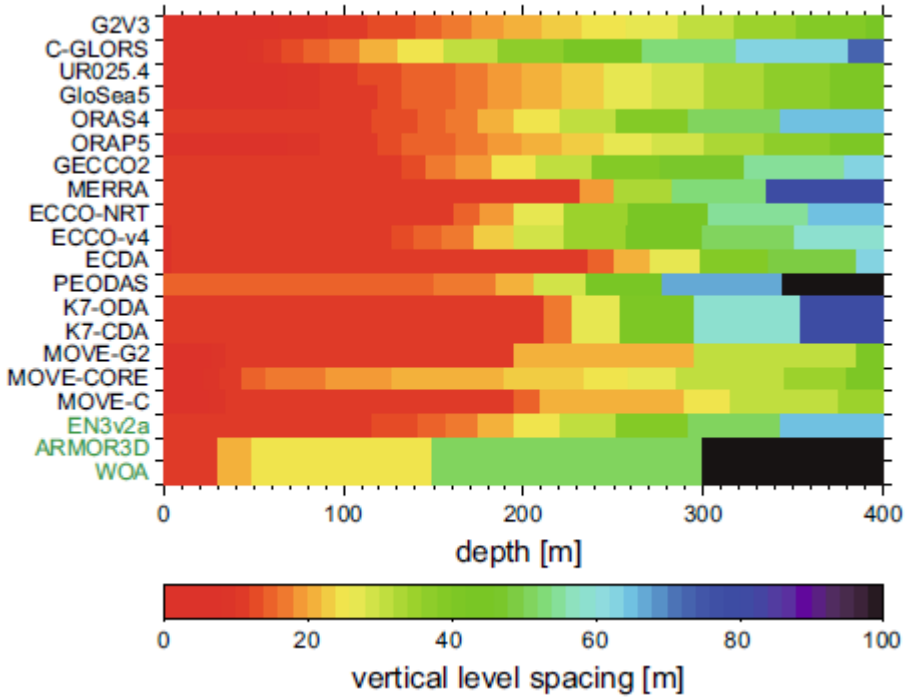

882

883 **Fig. 4** Vertical resolution of the syntheses in the ORA-IP.

884

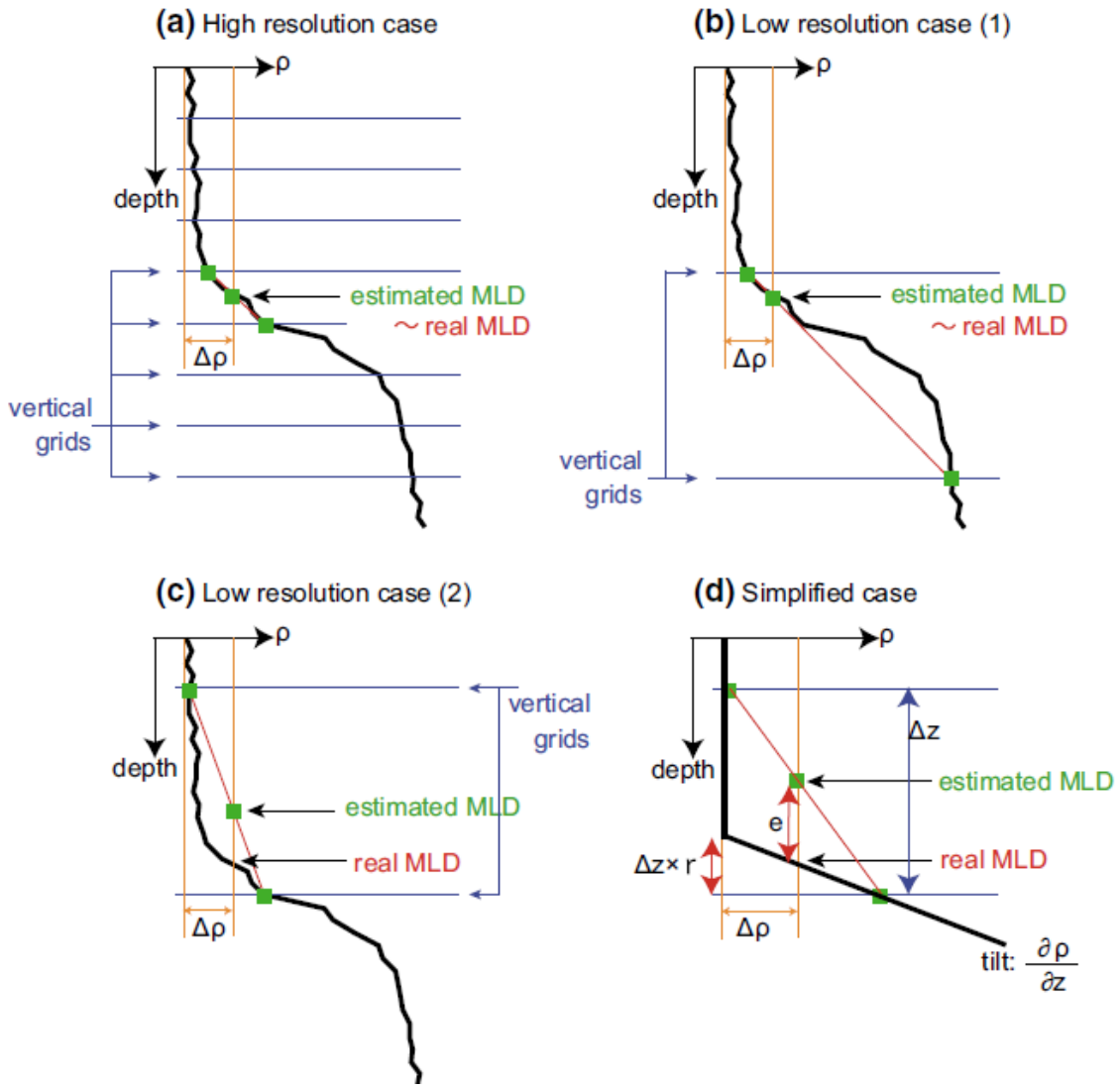

885

886 **Fig. 5** Schematic illustrations of the MLD estimation for (a) high resolution and (b, c) low

887 resolution cases. MLDs are estimated from a common vertical profile of potential density (black

888 line) by using linearly interpolated values between the vertical grids. (d) A simplified sketch

889 showing relationship between error in the MLD estimation and vertical level spacing.

890

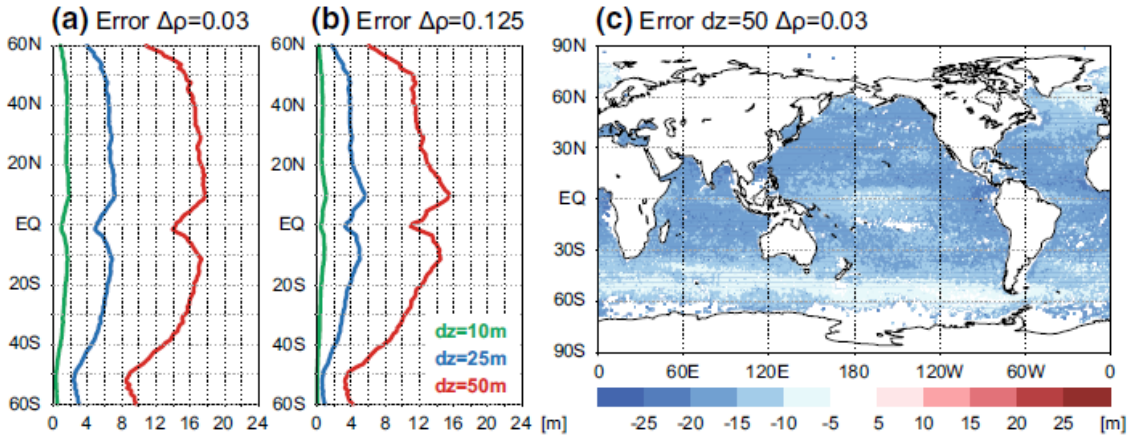

Fig. 6 (a, b) Zonal mean expected values for the underestimation associated with limited vertical resolution of profiles in the MLD estimation by using the criteria, $\Delta\rho = 0.03$ (a) and $\Delta\rho = 0.125$ kg m^{-3} (b). Green, blue and red lines denote the vertical resolutions of Δz =10, 25 and 50 m, respectively. (c) Distribution of the errors when $\Delta\rho = 0.03$ kg m^{-3} and Δz =50 m. $\frac{\partial \rho}{\partial z}$ values at the ML bottom are calculated from the individual Argo profiles over the 2000-2012 period and averaged onto monthly and 1 degree by 1 degree bins for use in Eq. (1). Units are in meter.

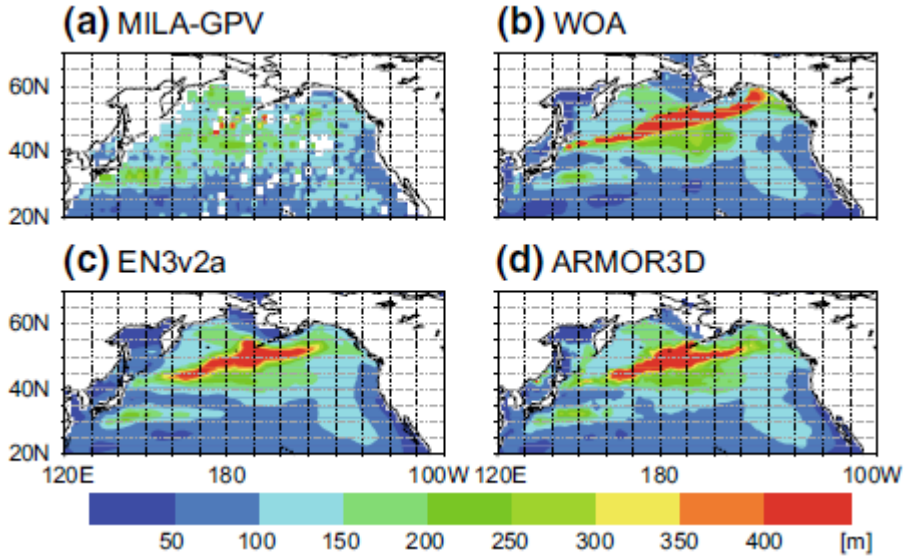

Fig. 7 ILDt05 distributions in March in the North Pacific basin averaged over 2001-2011 for (a)

902 MILA-GPV, (b) WOA, (c) EN3v2a and (d) ARMOR3D.

903

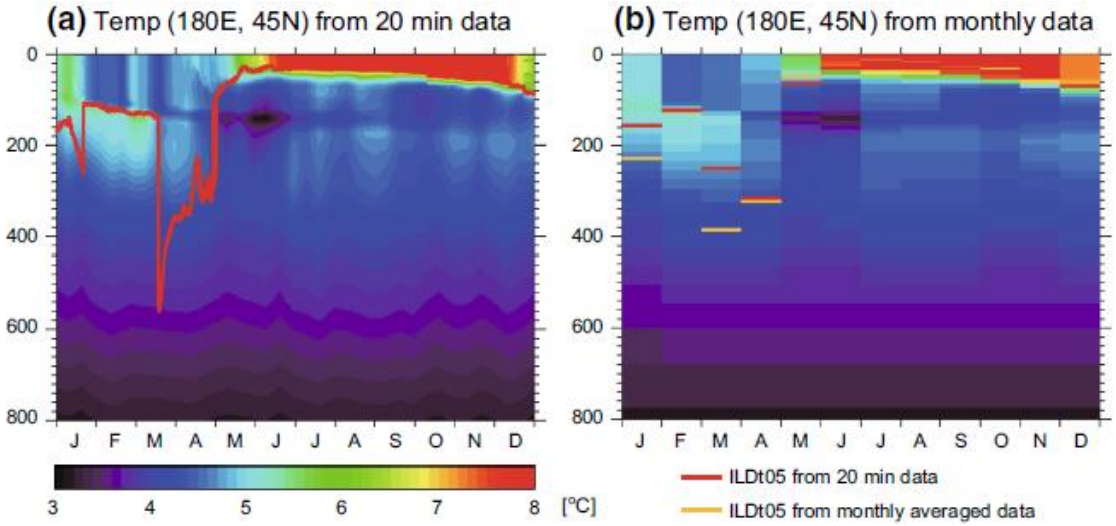

904

905 **Fig. 8** Time evolution of the vertical temperature profile in the subpolar North Pacific at 180ºE,

906 45ºN in 2001 represented (a) by snapshot data with an interval of the model time step (20

907 minute) and (b) by monthly mean data. Both time series are derived from the MOVE-G2

908 product. Red (yellow) line indicates ILDt05s calculated from the former (latter) data.

909

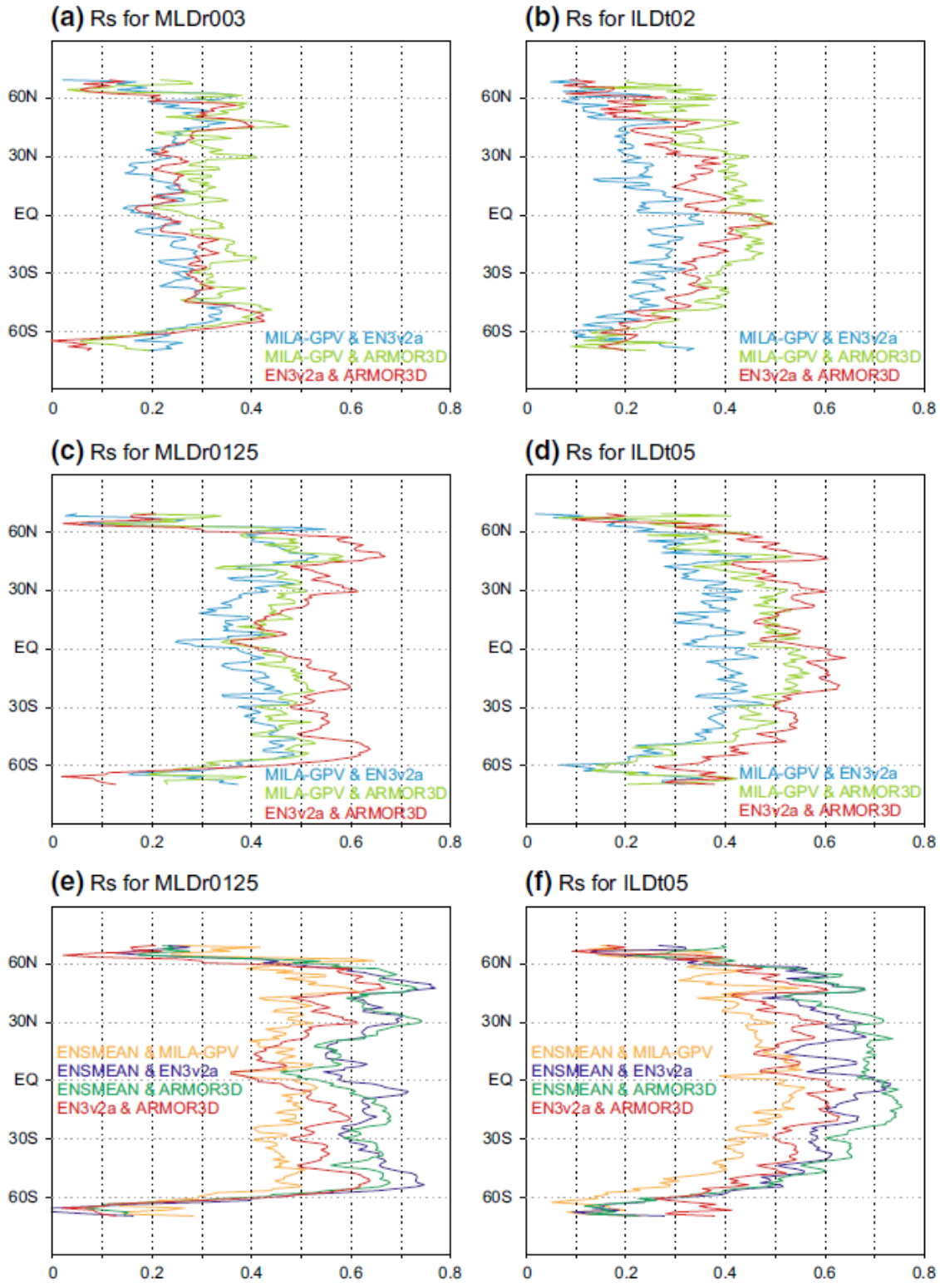

910

911 **Fig. 9** Zonal mean correlation coefficients of monthly interannual anomalies during 2005-2010

912 (defined in this study as monthly data over 6 years with the mean seasonal cycle for this period

removed), (a-d) among MILA-GPV, EN3v2a and ARMOR3D and (e, f) between ENSMEAN and MILA-GPV/EN3v2a/ARMOR3D, for (a) MLDr003, (b) ILDt02, (c, e) MLDr0125 and (d, f) ILDt05. The period was chosen because all datasets are available during this period.

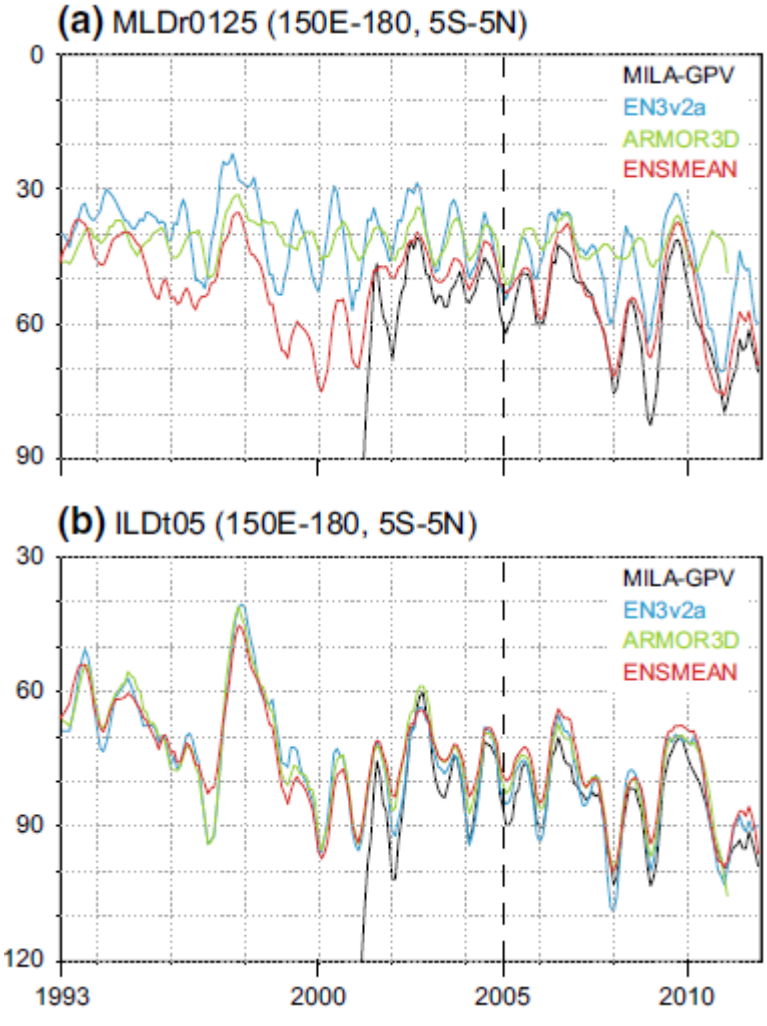

Fig. 10 Time series of MLDr0125s (a) and ILDt05s (b) averaged over the western Pacific warm pool region (150ºE-180º, 5ºS-5ºN) for MILA-GPV, EN3v2a, ARMOR3D and ENSMEAN (black, blue, green and red lines, respectively). 5-month running mean values are plotted.

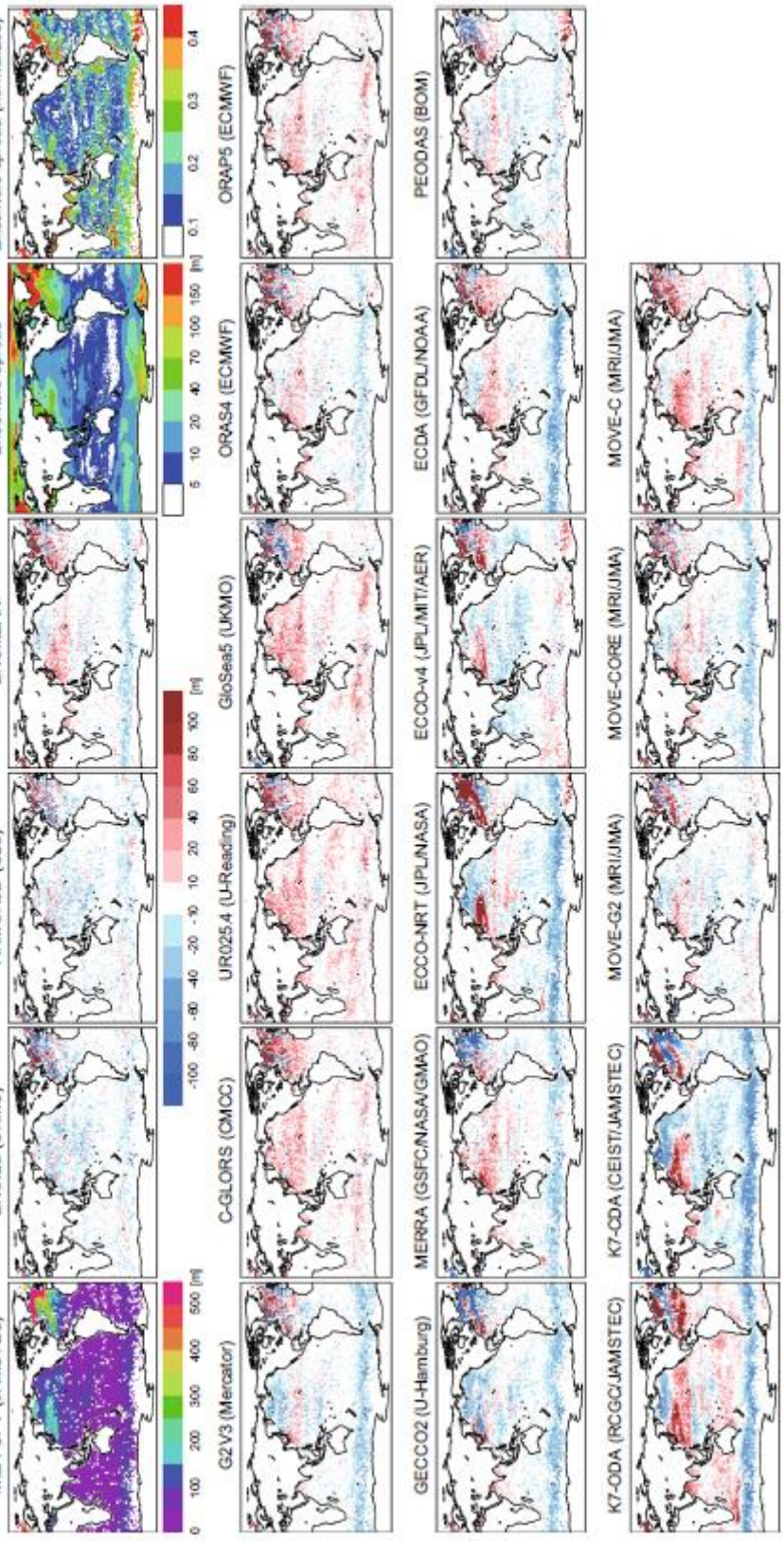

922

923 **Fig. 11** Distributions of MLDr0125 in February averaged over 2001-2011 for (top row from

924 left) MILA-GPV, differences between MILA-GPV and either EN3v2a, ARMOR3D or
925 ENSMEAN (e.g., EN3v2a−MILA-GPV), absolute and normalized (by the MILA-GPV values)
926 ensemble spread of the reanalyses and (others) differences between MILA-GPV and the
927 individual reanalyses.
928

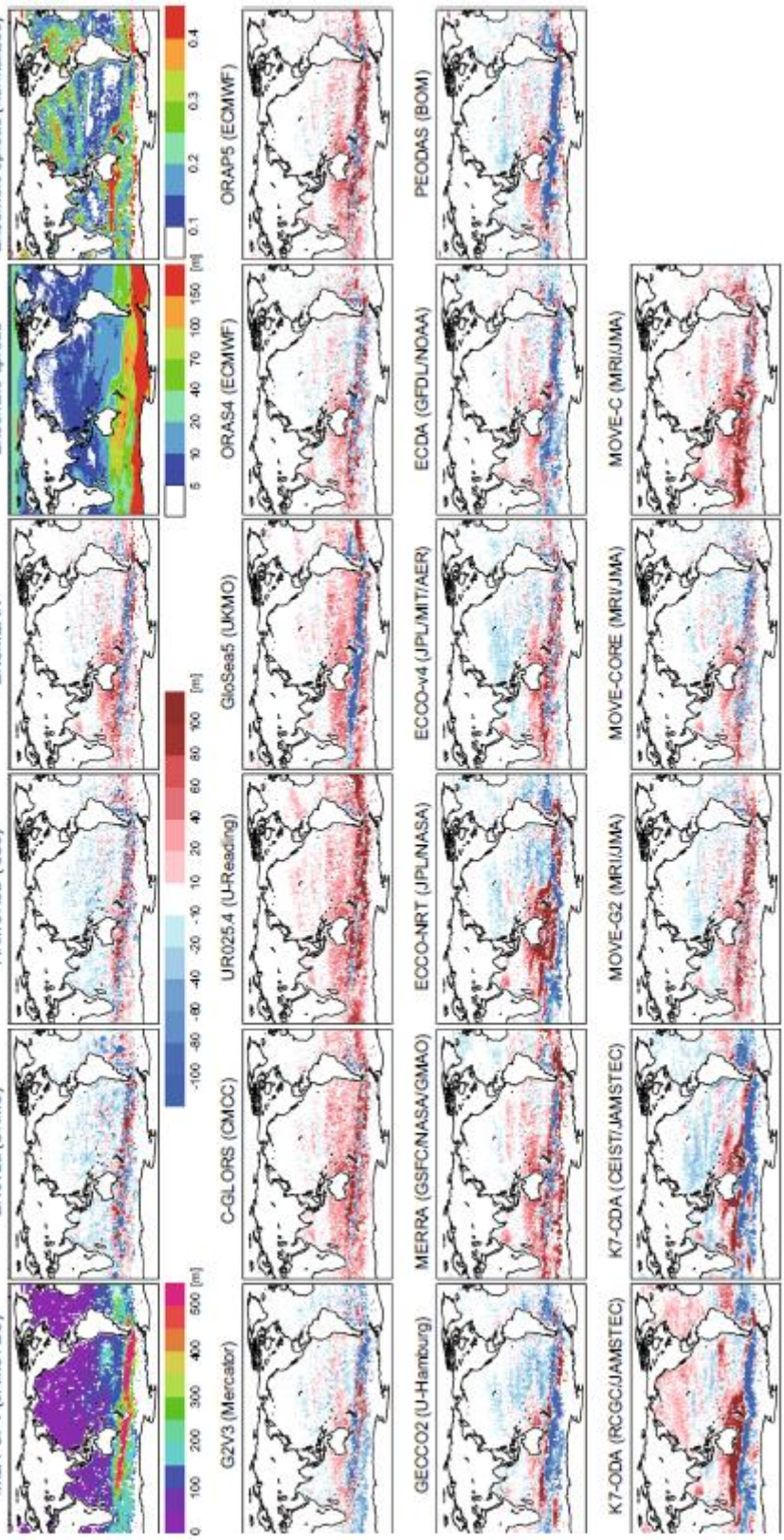

Fig. 12 Same as Fig. 11 but for August.

931

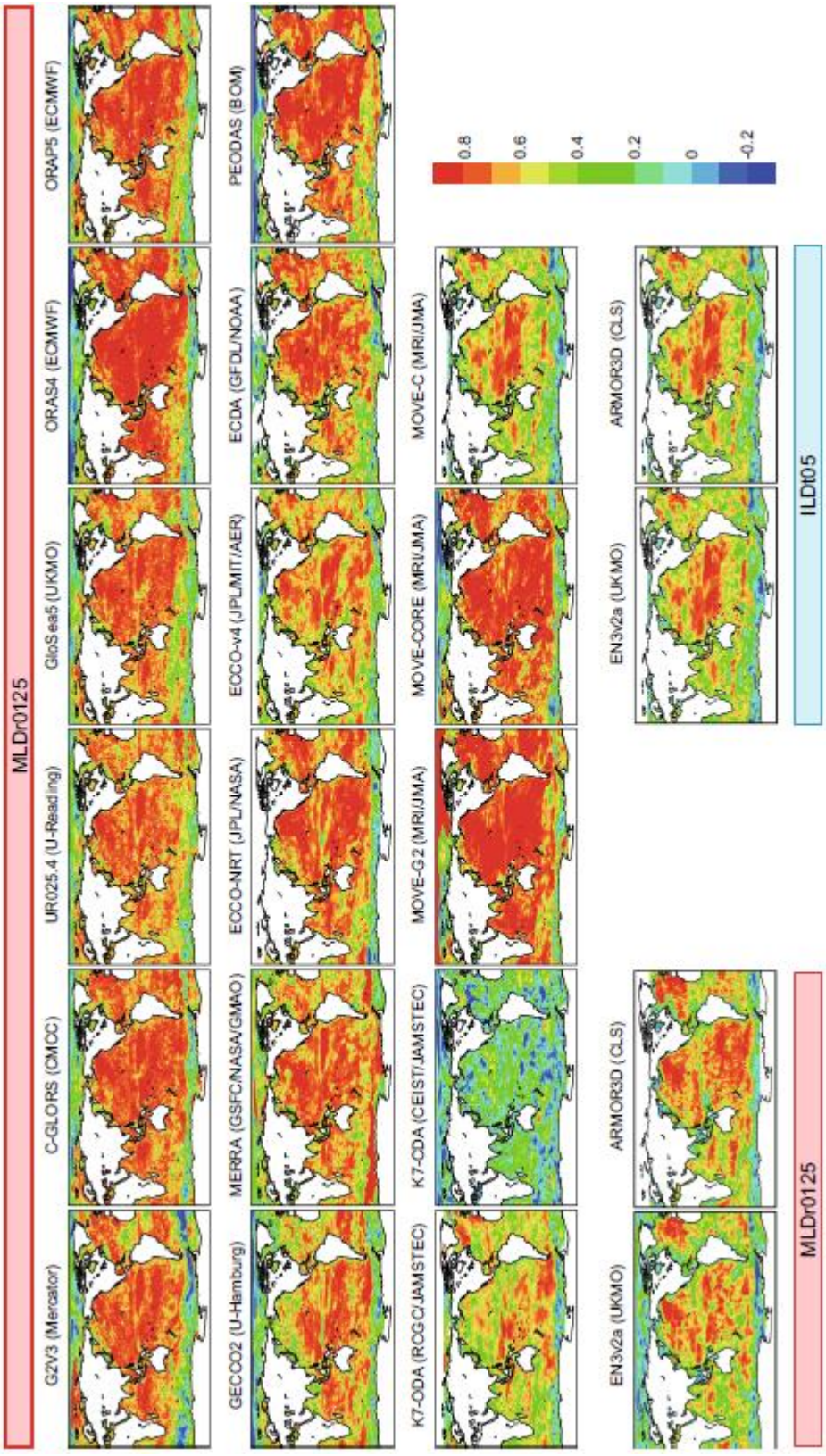
MLDr0125
G2V3 (Mercator)
C-GLORS (CMCC)
UR025.4 (U-Reading)
GloSea5 (UKMO)
ORAS4 (ECMWF)
ORAP5 (ECMWF)
GECCO2 (U-Hamburg)
MERRA (GSFC/NASA/GMAO)
ECCO-NRT (JPL/NASA)
ECCO-v4 (JPL/MIT/AER)
ECDA (GFDL/NOAA)
PEODAS (BOM)
K7-ODA (ROC/JAMSTEC)
K7-ODA (CEIST/JAMSTEC)
MOVE-G2 (MRI/JMA)
MOVE-CORE (MRI/JMA)
MOVE-C (MRI/JMA)
EN3v2a (UKMO)
ARMOR3D (CLS)
EN3v2a (UKMO)
ARMOR3D (CLS)
0.8
0.6
0.4
0.2
0
-0.2
ILDt05
MLDr0125

932

933 **Fig. 13** Distributions of correlation coefficients for the interannual anomalies of MLDr0125
934 over the 2001-2011 period between ENSMEAN and the individual reanalyses (1st-3rd rows)
935 and between ENSMEAN and EN3v2a/ARMOR3D (for both MLDr0125 and ILDt05; bottom
936 row).
937

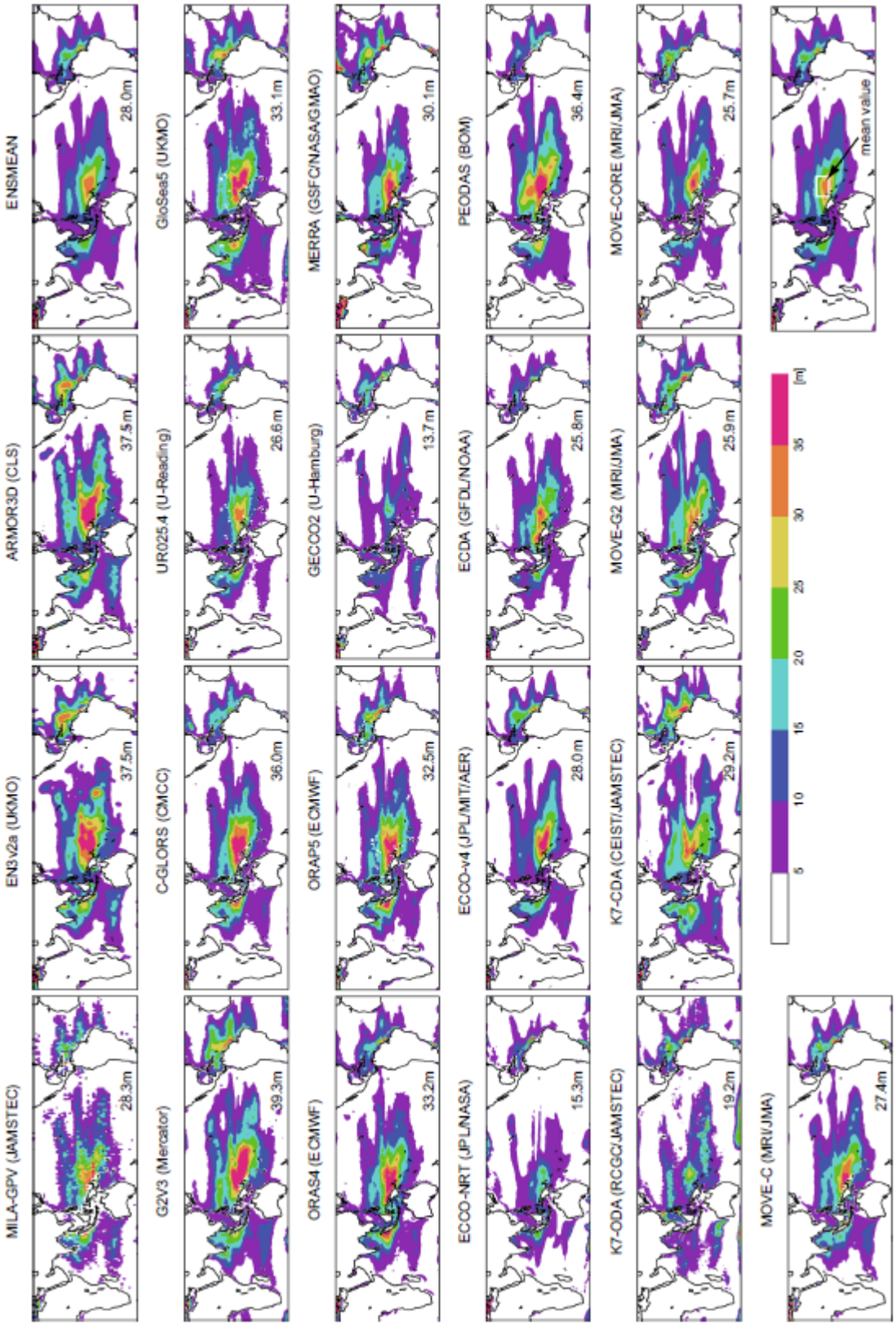

938

939 **Fig. 14** Distributions of BLT averaged over 2001-2011. BLT value averaged over the western

940 equatorial Pacific (150ºE-170ºE, 5ºS-5ºN; white box in the right bottom figure) is indicated in

941 each figure.

942

Table 1 Description of the observation-only analyses in the ORA-IP

Name	Center	Resolution	Assimilationed data	Reference
EN3v2a	UKMO	1^{O}, 30lv	TS	Ingleby and Huddleston (2007)
ARMOR3D	CLS	$1/3^{O}$, 33lv	TS/SLA/SST	Guinehut et al. (2012)

Table 2 Description of the reanalysis products in the ORA-IP

Name (Center)	OGCM Resolution	Forcing	ML model	Assimilation data	Assimilation Method	Reference
G2V3 (Mercator Océan)	NEMO3.1 1/4º, 75lv	ERAi corrected	Blanke and Delecluse (1993)	TS/SLA/SST/SIC	KF, 3DVAR, Bias,FGAT,IAU	Ferry et al. (2012)
C-GLORS (CMCC)	NEMO3.2 1/2º, 50lv	ERAi corrected	Blanke and Delecluse (1993)	TS/SLA/SST/SIC	3DVAR, FGAT	Storto et al. (2011)
UR025.4 (U-Reading)	NEMO3.2 1/4º, 75lv	ERAi	Blanke and Delecluse (1993)	TS/SLA/SST/SIC	OI, FGAT, IAU	Haines et al. (2012)
GloSea5 (UKMO)	NEMO3.2 1/4º, 75lv	ERAi	Blanke and Delecluse (1993)	TS/SLA/SST/SIC	3DVAR, FGAT, IAU	Blockley et al. (2013)
ORAS4 (ECMWF)	NEMO3.0 1ºx(0.3-1)º, 42lv	ERA40, ERAi	Blanke and Delecluse (1993)	TS/SLA/SST	3DVAR, FGAT, Bias, IAU	Balmaseda et al. (2013)
ORAP5 (ECMWF)	NEMO3.4 1/4º, 75lv	ERAi	Blanke and Delecluse (1993)	TS/SLA/SST/SIC	3DVAR, FGAT, Bias, IAU	Zuo et al. (2014)
GECCO2 (U-Hamburg)	MITgcm 1ºx(1/3-1)º, 50lv	NCEP-R1 corrected	Large et al. (1994)	TS/SLA/MDT/ SST	4DVAR	Köhl (2014)

MERRA (Ocean) (GSFC/NASA/GMAO)	MOM4 1/2ºx(1/4-1/2)º, 40lv	Merra	Large et al. (1994)	TS/SLA/SST/SIC	EnOI	Vernieres et al. (2012)
ECCO-NRT (JPL/NASA)	MITgcm 1ºx(0.3-1)º, 46lv	NCEP-R1 corrected	Large et al. (1994)	T/SLA	KF, KS	Fukumori (2002)
ECCO-v4 (JPL/MIT/AER)	MITgcm 0.4ºx(0.4-1)º, 50lv	ERAi corrected	Large et al. (1994)	TS/SLA/SST/SIC	4DVAR	Wunsch and Heimbach (2013)
ECDA (GFDL/NOAA)	MOM4 coupled 1ºx(0.3-1)º, 50lv	Coupled	Large et al. (1994)	TS/SST	EnKF	Chang et al. (2013)
PEODAS (BOM)	MOM2 2ºx(0.5-1.5)º, 25lv	ERA40, NCEP-R2	Chen et al. (1994)	TS/SST	EnKF	Yin et al. (2011)
K7-ODA (ESTOC) (RCGC/JAMSTEC)	MOM3 1º, 45lv	NCEP-R1 corrected	Large et al. (1994)	TS/SLA/SST	4DVAR	Masuda et al. (2010)
K7-CDA (CEIST/JAMSTEC)	MOM3 coupled 1º, 45lv	Coupled	Noh et al. (2005)	TS/SLA/SST	4DVAR	Sugiura et al. (2008)
MOVE-G2 (MRI/JMA)	MRI.COM3 1ºx(0.3-0.5)º, 53lv	JRA55 corrected	Noh et al. (2005)	TS/SLA/SST	3DVAR, FGAT, IAU	Toyoda et al. (2013)
MOVE-CORE (MRI/JMA)	MRI.COM3 1ºx0.5º, 51lv	CORE2	Umlauf and Burchard (2003)	TS	3DVAR, IAU, Bias	Danabasoglu et al. (2013)
MOVE-C (MRI/JMA)	MRI.COM2 1ºx(0.3-1)º, 50lv	Coupled	Noh et al. (2005)	TS/SLA/SST	3DVAR, IAU, Bias	Fujii et al. (2009)

Abbreviations: MDT (mean dynamic topography), KF (Kalman filter), 3DVAR (3 dimensional variational method), Bias (one-step bias-correction algorism), FGAT (first guess at appropriate time), 4DVAR (4 dimensional variational method), EnOI (ensemble optimal interpolation), KS (Kalman smoother), EnKF (ensemble KF), IAU (incremental analysis updates)

Table 3 Variables and duration available for the ORA-IP and contact parson

Synthesis	Variables	Duration	Contact parson
EN3v2a	All	1993-2011	S. Good
ARMOR3D	All	1993-2010	S. Guinehut
G2V3	All	1993-2011	F. Hernandez
C-GLORS	All	1991-2011	A. Storto
UR025.4	MLDr003, MLDr0125, ILDt05	1993-2010	M. Valdivieso
GloSea5	All	1993-Jul. 2012	M. Martin
ORAS4	All	1958-2011	M. Balmaseda
ORAP5	All	1993-2012	H. Zuo
GECCO2	All	1948-Nov. 2011	A. Köhl
MERRA	MLDr0125, ILDt05	1993-2011	G. Vernieres
ECCO-NRT	MLDr0125, ILDt05	1993-2011	O. Wang
ECCO-v4	MLDr0125, ILDt05	1992-2010	X. Wang
ECDA	All	2005-2011	Y.-S. Chang
PEODAS	All	1980-2012	O. Alves
K7-ODA	All	1975-2011	S. Masuda
K7-CDA	All	2000-2006	Y. Ishikawa
MOVE-G2	All	1993-2012	T. Toyoda
MOVE-CORE	All	1948-2007	Y. Fujii
MOVE-C	All	1950-2011	Y. Fujii

Durations submitted to the ORA-IP are sometimes shorter than those of the original reanalyses